Technische Universität München

Faculty of Mathematics
Chair for Applied Geometry and Discrete Mathematics

On the Tomography of Discrete Structures:

Mathematics, Complexity, Algorithms, and its Applications in Materials Science and Plasma Physics

Cumulative Habilitation Thesis by Andreas Alpers

Mentors: Prof. Dr. Peter Gritzmann
Prof. Dr. Rupert Lasser
Prof. Henning Friis Poulsen, Ph.D.

Acknowledgements

First and foremost, I would like to express my deepest thanks to my mentor Peter Gritzmann. Your support, encouragement, and inspiration in all phases of my academic career have been invaluable to me.

I would also like to thank Ruppert Lasser and Henning Friis Poulsen for serving on my habilitation committee.

Many thanks are due to my coauthors, discussion partners, and all those that have commented on the papers that serve as a basis for this work. In particular, I would like to thank Marcus Aldén, Kees Joost Batenburg, Chris Boothroyd, René Brandenberg, Andreas Brieden, Ran Davidi, Rafal E. Dunin-Borkowski, Hannes Ebner, Sandra Ebner-Fraß, Andreas Ehn, Jinming Gao, Richard J. Gardner, Viviana Ghiglione, Peter Gritzmann, Carl Georg Heise, Gabor T. Herman, Melanie Herzog, Lothar Houben, Ivan Kazantsev, Fabian Klemm, Erik Bergbäck Knudsen, Stefan König, Arun Kulshreshth, Yukihiro Kusano, Barbara Langfeld, David G. Larman, Erik Mejdal Lauridsen, Zhongshan Li, Hstau Liao, Allan Lyckegaard, Bernardo González Merino, Dmitry Moseev, Robert S. Pennington, Andreas Pitschi, Henning Friis Poulsen, Wolfgang Ferdinand Riedl, Michael Ritter, Lajos Rodek, Mirko Salewski, Søren Schmidt, Felix Schmiedl, Martin Schwenk, Anastasia Shakhshneyder, Matthias Silbernagl, Paul Stursberg, Anusch Taraz, Robert Tijdeman, and Jiajian Zhu.

I was supported in this research by various grants and institutions. In addition to the support provided by the "Lehrstuhl" of Peter Gritzmann, I gratefully acknowledge the support from the German Science foundation for the project "Geometric reconstruction in refraction- and diffraction-based tomography" (AL 1431/1-1), the Feodor Lynen Scholarships, the Walter von Dyck-Preis (TU München), and the European COST Network MP1207.

Moreover, I would like to thank Gabor T. Herman (City University of New York, USA), Leslie E. Trotter, Jr. (Cornell University, USA), Dorte Juul Jensen (Risø DTU National Laboratory, Denmark), Henning Friis Poulsen (Technical University of Denmark, Denmark), and Per Christian Hansen (Technical University of Denmark, Denmark) for supporting and hosting me at their respective institutions.

Last but not least, I would like to thank my family. Without my parents, siblings, my wife Susann, and daughter Olivia this work would not have been possible. To you, I dedicate this thesis.

Contents

1 Introduction **5**
- 1.1 General Notation . . . 6
- 1.2 Grains, Nanowires, Microparticles . . . 7

2 Aspects of Diophantine Number Theory in Tomography, [H5, H9, H12] **8**
- 2.1 Theory . . . 8
  - 2.1.1 The PTE Problem: History and Notation . . . 9
  - 2.1.2 Results from [H12] . . . 12
  - 2.1.3 Results from [H9] . . . 15
  - 2.1.4 Additional Comments On Switching Components . . . 17
  - 2.1.5 Results from [H5] . . . 18

3 Tomographic Super-Resolution Imaging, [H4] **22**
- 3.1 Algorithms and Complexity . . . 22
  - 3.1.1 Results from [H4] . . . 22

4 Tomographic Point Tracking: Theory and Applications, [H3, H6, H7, H14] **26**
- 4.1 Theory . . . 26
  - 4.1.1 Results from [H3] . . . 26
  - 4.1.2 Results from [H6] . . . 27
  - 4.1.3 Results from [H7] . . . 30
- 4.2 Applications . . . 33
  - 4.2.1 Plasma Physics: Results from [H14] . . . 33

5 Tomographic Reconstructions of Polycrystals, [H1, H8, H10, H11, H13] **35**
- 5.1 Theory, Algorithms, and Applications . . . 35
  - 5.1.1 Geometric Clustering, [H1] . . . 35
  - 5.1.2 Stochastic Algorithms, [H10, H11, H13] . . . 39
  - 5.1.3 Fourier Phase Retrieval, [H8] . . . 43

6 Geometric Methods for Electron Tomography, [H2] **46**
- 6.1 Algorithms and Applications in Materials Science . . . 46
  - 6.1.1 Results from [H2] . . . 47

Papers Included in This Thesis **49**

Other References **51**

Index **69**

THESIS SUMMARY

1 Introduction

This habilitation thesis is a collection of 11 peer-reviewed journal papers [H1, H2, H5, H6, H7, H8, H9, H10, H12, H13, H14], one book chapter [H11], and two submitted papers [H3, H4]. In the following, I will give an integrated view of these papers.

Apart from the Introduction there are five sections, representing five research topics, in this thesis: (i) Aspects of Diophantine Number Theory in Tomography, (ii) Tomographic Super-Resolution Imaging, (iii) Tomographic Point Tracking: Theory and Applications, (iv) Tomographic Reconstructions of Polycrystals, and (v) Geometric Methods for Electron Tomography.

The research topics are motivated by different tomographic applications in materials science and plasma physics. For each of the topics (i)-(iv) a deeper mathematical theory had to be developed, in order to devise problem-specific algorithms. The mathematical areas to which I contributed are listed (along with the papers and applications) in the following table.

Paper(s)	Mathematics	Application
[H12]	diophantine number theory, algebra	tomography
[H9]	diophantine number theory, combinatorics	tomography
[H5]	diophantine number theory, complexity, discrete optimization	discrete tomography
[H4]	combinatorics, discrete optimization, complexity	super-resolution
[H3, H6, H7, H14]	discrete optimization, complexity, combinatorics	plasma physics
[H1]	geometric clustering, discrete optimization	materials science
[H10, H11, H13]	Markov processes	materials science
[H8]	Fourier phase retrieval	materials science
[H2]	geometric tomography	materials science

Table 1: Mathematics and Applications. Overview of the respective content of the papers contained in this thesis.

The work presented in this thesis is of an interdisciplinary nature. This reflects in the choice of international journals in which I published.

- *Mainly mathematical content:* SIAM Journal on Discrete Mathematics, Journal of Number Theory, Bulletin of the London Mathematical Society;
- *Mainly algorithmic content:* Philosophical Magazine, Inverse Problems and Imaging, Computational Physics Communications;
- *Mainly application content:* Applied Physics Letters, Ultramicroscopy, Journal of Applied Crystallography, Journal of the Optical Society of America A.

The interdisciplinary nature is also reflected by the fact that, next to mathematics, my work has been cited in journals from *computer science*, *materials science*, *physics*, *chemistry*, and *nanoscience*. According to their authors, several PhD theses in mathematics were motivated by some of my work (see, e.g., the theses [43, 200] from the University of Waterloo and the University of Illinois at Urbana-Champaign, respectively, in which generalizations of the problem introduced in [H12] are studied; see also Sect. 2).

Moreover, several of the developed algorithms in my work have already been used on real-data by physicists and materials scientists, others need to wait until the technological facilities have been commissioned. An example for the latter is [H8], which, in the Conceptual Design Report [159] of the *European X-ray free-electron laser (European XFEL)* [70], has been identified as being of potential use in experiments to be performed with the novel *Materials Imaging and Dynamics (MID)* instrument [71].

1.1 General Notation

Throughout this thesis, $\mathbb{Z}$, $\mathbb{R}$, $\mathbb{N} = \{1, 2, \ldots\}$, and $\mathbb{Z}[i]$ denote the sets of integers, reals, natural numbers, and Gaussian integers, respectively. Further, we set $\mathbb{N}_0 := \mathbb{N} \cup \{0\}$, and $\mathbb{K} \in \{\mathbb{R}, \mathbb{Z}\}$. The symbol i will be used to denote the imaginary unit in the complex numbers. The algebra of quaternions will be denoted by $\mathbb{H}$.

For $k \in \mathbb{N}$ we set $k\mathbb{N}_0 := \{kj : j \in \mathbb{N}_0\}$, $[k] := \{1, \ldots, k\}$, and $[k]_0 := \{0, \ldots, k\}$. The linear span of a vector v is denoted by $\mathrm{lin}(v)$. By $|X|$ we denote the cardinality of the set X or the absolute value of the number X. If $\xi \in \mathbb{R}$, then $\lceil \xi \rceil$ denotes the smallest integer greater than or equal to ξ.

With $\mathbb{P}$ we denote the complexity class that contains all decision problems that can be solved in polynomial time by a deterministic Turing machine. The class of decision problems solvable in polynomial time by a theoretical non-deterministic Turing machine is denoted by $\mathbb{NP}$ (for background material on complexity theory, see, e.g., [91]).

The O-symbol has the usual meaning: $f(n) = O(g(n))$ means that $f(n)/g(n)$ is bounded as $n \to \infty$.

1.2 Grains, Nanowires, Microparticles

In several of our papers we are utilizing real-word data, which is typically obtained by synchrotron X-ray diffraction, electron microscopes, or high-speed cameras. The corresponding real-world objects in these cases are the so-called *grains*, *nanowires*, and *microparticles*, respectively. In the following we briefly introduce these objects (illustrative examples are shown in Fig. 1). The interested reader can find more information in the monographs [5, 196, 245].

Many materials – in particular most metals, ceramics and alloys – are *polycrystalline materials*, which means that they are comprised of a set of small crystals. These small crystals, typically $10 - 100$ micrometer in diameter, are known as *grains*. Each grain is characterized by its center of mass, shape and internal lattice structure (note that a reconstruction is usually not performed on the atomic level). Since the geometric features of the grains within the *polycrystal* determine most of the material's physical, chemical and mechanical properties, it is the study of grains that is of central importance in many areas of materials science (see, e.g. [196]). Fig. 1(a) shows a *grain map* (i.e., an image of a polycrystal). The grains are depicted in different colors. We remark that grain studies, e.g. on crack corrosion [136], responses to stress [123, 163], and grain growth phenomena [180, 211], require techniques to probe grain complexes deep inside of bulk materials. Over the past two decades two tomography-based experimental techniques have emerged, which utilize high-energetic X-rays as produced by *third-generation synchrotrons* (as, for instance, the European synchrotron radiation facility, ESRF, in Grenoble, France). These tomography-based techniques are known as *3-dimensional X-ray diffraction (3DXRD)* [192] and *diffraction contrast tomography (DCT)* [156]. Some of our work is based on such data. State-of-the-art surveys can be found in [21, 191, 192, 202].

In [H2] we consider *nanowires*. These small wires that are tens of nanometers in diameter and micrometers in length, are promising building blocks for future electronic and optical devices; see [152, 175]. They are typically grown from a substrate and much research effort is being focused on understanding and controlling their growth mechanisms [61]. Electron tomography, as in various materials science applications, is rapidly developing into a powerful 3D imaging tool for studying these effects at the nanoscale [20, 174]. We report on this in connection with our paper [H2]. An image depicting an indium arsenide nanowire is shown in Fig. 1(b).

In [H14] we reconstruct the trajectories of several titanium dioxide (TiO_2) *microparticles* (which are about 3 micrometers in diameter). Titanium dioxide microparticles are often used as *tracer particle* in high-temperature flow experiments as TiO_2 is a ceramic material (further favorable properties of this material are discussed, for instance, in [167]). A high-speed camera image from our experiment in [H14], which depicts a

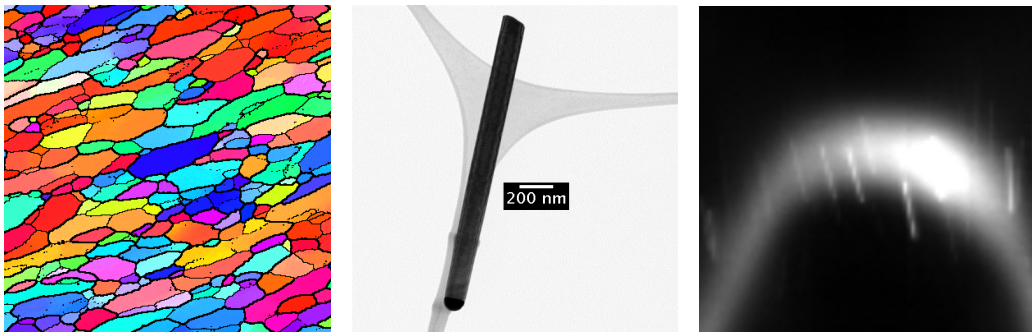

(a) **(b)** **(c)**

Figure 1: Images of real-world objects from our papers: (a) a grain map of an aluminum sample (here an EBSD image is shown), (b) an InAs nanowire (here a bright-field TEM image is shown), (c) TiO_2 microparticles near a gliding arc discharge (here an optical high-speed camera image is shown).

gliding arc discharge and several vertically moving TiO_2 microparticles (appearing as 'streaks'), is shown in Fig. 1(c).

2 Aspects of Diophantine Number Theory in Tomography, [H5, H9, H12]

2.1 Theory

In the following we discuss the *Prouhet-Tarry-Escott (PTE) problem* from Diophantine number theory. The PTE problem can be stated as follows.

Problem 1 (Prouhet, 1851; Tarry, 1912; Escott, 1910).
Given two natural numbers k and n. Find two different multisets $X := \{\xi_1, \ldots, \xi_n\} \subseteq \mathbb{Z}$ and $Y := \{\eta_1, \ldots, \eta_n\} \subseteq \mathbb{Z}$, such that

$$\xi_1^j + \xi_2^j + \ldots + \xi_n^j = \eta_1^j + \eta_2^j + \ldots + \eta_n^j, \qquad \text{for } j \in [k]. \tag{1}$$

Any pair (X, Y) that satisfies (1) is called a *solution of the PTE problem for* (k, n), and we will denote this by $X \overset{k}{=} Y$. For instance, it holds that

$$\{0, 4, 8, 16, 17\} \overset{4}{=} \{1, 2, 10, 14, 18\}.$$

The system (1) is a special class of multigrade equations [95, Sect. 1]. In the following we give a brief overview of the history of the PTE problem. Additional background information can be found in the monographs [34, 62, 95] and in [35].

2.1.1 The PTE Problem: History and Notation

The PTE problem can be traced back to a 1750 letter from Goldbach to Euler [97]. In this letter Goldbach states the identity

$$(\alpha+\beta+\delta)^2+(\alpha+\gamma+\delta)^2+(\beta+\gamma+\delta)^2+\delta^2 = (\alpha+\delta)^2+(\beta+\delta)^2+(\gamma+\delta)^2+(\alpha+\beta+\gamma+\delta)^2,$$

which holds for any $\alpha, \beta, \gamma, \delta \in \mathbb{Z}$, and hence

$$\{\alpha+\beta+\delta, \alpha+\gamma+\delta, \beta+\gamma+\delta, \delta\} \overset{2}{=} \{\alpha+\delta, \beta+\delta, \gamma+\delta, \alpha+\beta+\gamma+\delta\}.$$

Euler notices in his reply [69] that the case $\delta = 0$ is particularly simple ("ziemlich offenbar"). However, a later theorem by Frolov [80] implies that an arbitrary constant can be added to each number of a PTE solution, hence Euler's special case implies Goldbach's result. More generaly, it can be shown that if (X, Y) is a PTE solution for (k, n) and $f(t) = \alpha t + \beta$ is a linear transformation with $f(X), f(Y) \subseteq \mathbb{Z}$, then $(f(X), f(Y))$ is also a PTE solution for (k, n). In this case (X, Y) and $(f(X), f(Y))$ are called *equivalent solutions*.

The PTE problem is named after Prouhet [197], Escott [68], and Tarry [230]. It was already known to them that for every k there exist PTE solutions for $(k, n) = (k, 2^k)$; see [242] and [62, Sect. 24]. A straightforward procedure to generate such solutions is as follows. Express each $p \in [2^{k+1} - 1]_0$ as a binary number. If this binary expression of p contains an even number of 1's, then assign p to the set X, otherwise to Y. Then, (X, Y) with $X =: \{\xi_1, \ldots, \xi_{2^k}\}$ and $Y =: \{\eta_1, \ldots, \eta_{2^k}\}$ is a PTE solution for $(k, n) = (k, 2^k)$. Proofs of this result can be found, for instance, in [178, 242]. For generalizations see [148, 219].

On the other hand, there are no PTE solutions for (k, n) if $n < k + 1$. This result, which is straightforward to prove by means of Newton's identities [110, Sect. 21.9], is commonly attributed to Bastien [23]. PTE solutions for $(k, n) = (k, k + 1)$ are called *ideal solutions*, and it is an open question whether they exist for any k. While Wright conjectured in [241] that the answer is affirmative, other authors pointed to the fact that newer heuristic arguments seem to suggest a negative answer (see, e.g, [34, Sect. 11]). At present, ideal solutions are only known for $k \in [11] \setminus \{10\}$. In fact, infinitely many non-equivalent solutions are known for every $k \in [11] \setminus \{8, 10\}$ (see [34, Sect. 11] and [51]), while for $k = 8$ only two non-equivalent ideal solutions are known (see [36]).

In 1935, Wright [241] showed that for every k there exist PTE solutions for (k, n) with $n \leq \frac{1}{2}(k^2 + k + 2)$. The current best bound on n, which is due to Melzak [168], guarantees existence of PTE solutions for (k, n) with $n \leq \frac{1}{2}(k^2 - 3)$ if k is odd and $n \leq \frac{1}{2}(k^2 - 4)$ if k is even. None of these proofs of bounds on n that depend polynomially on k are constructive.

The PTE problem has many connections to other problems, including the *"easier" Waring problem* [240, 243], [34, Sect. 12], the *Hilbert-Kamke problem* [128, 137], and a conjecture of Erdős and Szekeres [52, 67, 162], [34, Sect. 13]. In addition, there are connections to Ramanujan identities [166, 184], other types of multigrade equations [49, 220], problems in algebra [161, 176], geometry [76], combinatorics [3, 6, 30], graph theory [118], and computer science [31, 45, 82].

There is also a connection between the PTE problem and tomography. As communicated by Gardner [65], a connection between general multigrades and discrete tomography has first been noted by Ron Graham (unpublished). The first published relation between the particular PTE problem and tomography seems to be contained in the present author's Ph.D. thesis [8, Sect. 6]. There, projections of so-called *switching components* (which will be explained further below) are shown to yield PTE solutions for specific values of (k, n).

Building upon [8, Sect. 6], we establish in [H12] a more direct connection between tomography and a generalization of the PTE problem. In fact, we introduce the more general *PTE_d problem*:

Problem 2 ([H12]).
Given natural numbers k, n, and d. Find two different multisets $X := \{\xi_1, \ldots, \xi_n\}$, $Y := \{\eta_1, \ldots, \eta_n\} \subseteq \mathbb{Z}^d$ with $\xi_l = (\xi_{l1}, \ldots, \xi_{ld})^T$, $\eta_l = (\eta_{l1}, \ldots, \eta_{ld})^T$ for $l \in [n]$ such that

$$\sum_{l=1}^{n} \xi_{l1}^{j_1} \xi_{l2}^{j_2} \cdot \ldots \cdot \xi_{ld}^{j_d} = \sum_{l=1}^{n} \eta_{l1}^{j_1} \eta_{l2}^{j_2} \cdot \ldots \cdot \eta_{ld}^{j_d}$$

for all non-negative integers $j_1, \ldots, j_d$ with $j_1 + j_2 + \ldots + j_d \leq k$.

Again, we write $X \stackrel{k}{=} Y$ for a solution. There are trivial ways of generating PTE_d-solution from PTE_1-solutions. For instance, if $\{\alpha_1, \ldots, \alpha_n\} \stackrel{k}{=} \{\beta_1, \ldots, \beta_n\}$ is a PTE_1-solution, then $\{\xi_1, \ldots, \xi_n\} \stackrel{k}{=} \{\eta_1, \ldots, \eta_n\}$ with $\xi_l := (\alpha_l, \ldots, \alpha_l)^T$ and $\eta_l := (\beta_l, \ldots, \beta_l)^T$, $l \in [n]$, is a solution to PTE_d. Such and other similarly trivial cases are in the following excluded from consideration.

Clearly, the PTE_d problem can be viewed as a higher-dimensional or multinomial version of the original PTE problem. Another natural generalization of the PTE problem is to consider other rings than the integers.

Problem 3 ([H12]).
Let R denote a ring. Given $(k, n) \in \mathbb{N}^2$. Find two different multisets $X := \{\xi_1, \ldots, \xi_n\}$, $Y := \{\eta_1, \ldots, \eta_n\} \subseteq R$, such that

$$\xi_1^j + \xi_2^j + \ldots + \xi_n^j = \eta_1^j + \eta_2^j + \ldots + \eta_n^j, \qquad \text{for } j \in [k]. \tag{2}$$

We call this here the *R-PTE problem*.

Obviously, any solution to the PTE_d problem is a solution to the $\mathbb{Z}^d$-PTE problem. Moreover, by considering the function $f : \mathbb{Z}^2 \to \mathbb{Z}[i]$, $(\xi_1, \xi_2)^T \mapsto \xi_1 + \xi_2 i$, we clearly have that any solution $X \overset{k}{=} Y$ to the PTE_2 problem yields a solution $f(X) \overset{k}{=} f(Y)$ to the $\mathbb{Z}[i]$-PTE problem. In [H12], and as we will explain below, we provide results and infinitely many non-equivalent ideal solutions for the PTE_2 problem (for $k \in \{1, 2, 3, 5\}$).

While, according to Caley [44]

> "Alpers and Tijdeman [H12] were the first to consider the PTE problem over a ring other than the integers,"

this line of research has in the meantime been taken up by other researches. In [50], Choudhry examines the PTE problem over the ring of 2×2 integer matrices. Prugsapitak studies in her Ph.D. thesis [200] and in [199] the PTE problem for $k = 2$ over quadratic number fields. Caley generalizes in his Ph.D. thesis [43] and in [44] several results on the constant arising from solutions to the PTE problem over quadratic number fields, and he provides the first ideal solution to the $\mathbb{Z}[i]$-PTE problem for $k = 10$. All ideal solutions to the $\mathbb{Z}[i]$-PTE problem for $k = 2$ are determined by Prugsapitak in [198]. In the case of the $\mathbb{F}_p$-PTE problem for $k = 2$, where $\mathbb{F}_p$ denotes a field of prime order p, the number of ideal solutions is determined in the 2014 paper [142] of Prugsapitak and Kongsiriwong.

We will now discuss the results of [H9, H12] in more detail. To this end we need to introduce some notation. Let $d \in \mathbb{N}$ with $d \geq 2$. We set

$$\mathcal{F}^d(\mathbb{K}) := \{F : F \subset \mathbb{K}^d \wedge F \text{ is finite}\},$$

and $\mathcal{F}^d := \mathcal{F}^d(\mathbb{Z})$. The elements of $\mathcal{F}^d$ are called *lattice sets*. Let $\mathcal{S}^d$ denote the set of all 1-dimensional linear subspaces of $\mathbb{R}^d$, and let $\mathcal{L}^d$ be the subset of $\mathcal{S}^d$ of all such subspaces that are spanned by vectors from $\mathbb{Z}^d$. The elements of $\mathcal{L}^d$ will be referred to as *lattice lines*. Further, for $S \in \mathcal{S}^d$ let $\mathcal{A}_{\mathbb{K}}(S) = \{v + S : v \in \mathbb{K}^d\}$. Then, for $F \in \mathcal{F}^d(\mathbb{K})$ and $S \in \mathcal{S}^d$, the *(discrete 1-dimensional) X-ray of F parallel to S* is the function

$$X_S F : \mathcal{A}_{\mathbb{K}}(S) \to \mathbb{N}_0$$

defined by

$$X_S F(T) = |F \cap T|,$$

for each $T \in \mathcal{A}_{\mathbb{K}}(S)$. Two sets $F_1, F_2 \in \mathcal{F}^d(\mathbb{K})$ are called *tomographically equivalent (with respect to $S_1, \ldots, S_m \in \mathcal{S}^d$)* if $X_{S_j} F_1 = X_{S_j} F_2$ for $j \in [m]$. We call any pair (F_1, F_2) of two different sets $F_1, F_2 \subseteq \mathbb{K}^d$ that are tomographically equivalent with respect to m different directions an *m-switching component (in $\mathbb{K}^d$)*. Clearly, we have $|F_1| = |F_2|$. We refer to $|F_1|$ as the *size of the switching component* (F_1, F_2). Several examples of switching components are shown in Fig. 2.

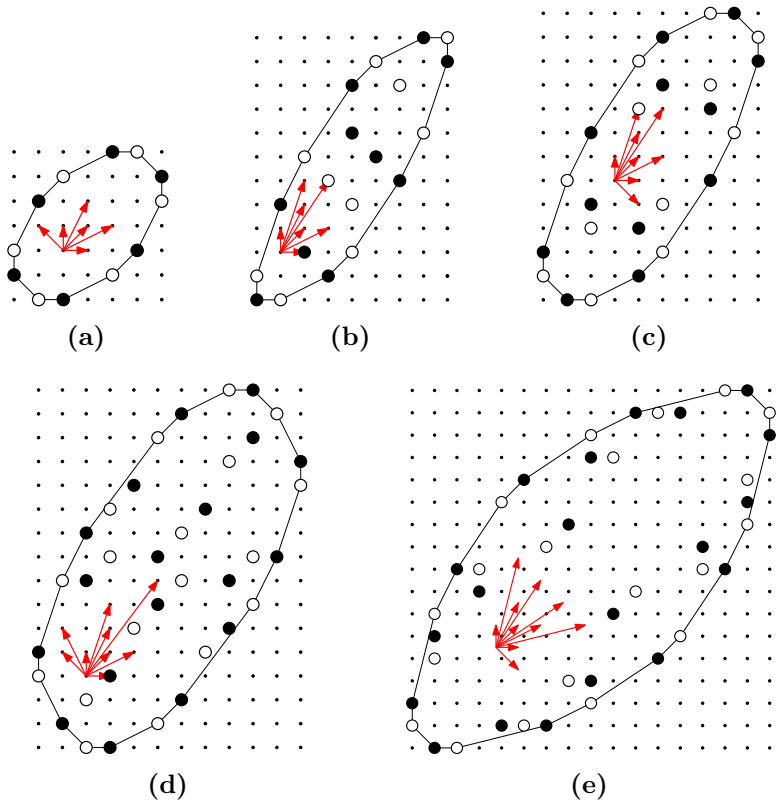

Figure 2: Small switching components for (a) $m = 6$, (b) $m = 7$, (c) $m = 8$, (d) $m = 9$, and (e) $m = 10$ directions (indicated in red). The switching components are pairs of 6, 10, 12, 18, and 20 black and white points, respectively.

2.1.2 Results from [H12]

A main result of [H12] is the following theorem that relates switching components to PTE_2 solutions.

Theorem 4. Any $(m+1)$-switching component (X, Y) in $\mathbb{Z}^2$ gives a PTE_2-solution

$$X \overset{m}{=} Y.$$

The proof of this theorem relies on a suitable encoding of points as polynomials. First, it can be shown [H12, Lem. 7] that each monomial $x^{j_1}y^{j_2}$, with $j_1 + j_2 = m$, can be expressed as a linear combination of the polynomials

$$(\beta_0 x - \alpha_0 y)^m, \ldots, (\beta_m x - \alpha_m y)^m \in \mathbb{Z}[x, y],$$

with $S_j := \operatorname{lin}\left((\alpha_j, \beta_j)^T\right)$, $j \in [m]$, denoting the $m+1$ directions of the switching component. Hence, there exist $\gamma_0, \ldots, \gamma_m \in \mathbb{R}$ with

$$x^{j_1} y^{j_2} = \sum_{j=0}^{m} \gamma_j (\beta_j x - \alpha_j y)^m. \tag{3}$$

Second, as on any line parallel to $\operatorname{lin}\left((\alpha_j, \beta_j)^T\right)$, $j \in [m]_0$, there are equally many points of X and Y, the multisets $\{(\beta_j \xi_{l1} - \alpha_j \xi_{l2}) : l \in [n]\}$ and $\{(\beta_j \eta_{l1} - \alpha_j \eta_{l2}) : l \in [n]\}$ are equal for any $j \in [m]_0$. With this, and by plugging the points of X and Y into (3), we obtain

$$\sum_{l=1}^{n} \xi_{l1}^{j_1} \xi_{l2}^{j_2} - \sum_{l=1}^{n} \eta_{l1}^{j_1} \eta_{l2}^{j_2} = \sum_{l=1}^{n} \sum_{j=0}^{m} \gamma_j (\beta_j \xi_{l1} - \alpha_j \xi_{l2})^m - \sum_{l=1}^{n} \sum_{j=0}^{m} \gamma_j (\beta_j \eta_{l1} - \alpha_j \eta_{l2})^m = 0,$$

which readily implies the claimed result (see proof of [H12, Thm. 8]).

With $\pi(X)$ denoting the projection of a set $X \subseteq \mathbb{Z}^2$ onto the first coordinate, we obtain directly the following corollary to Thm. 4 (see also [H12, Rem. 10]).

Corollary 5. Every $(m+1)$-switching component (X, Y) in $\mathbb{Z}^2$ gives a PTE_1-solution

$$\pi(X) \overset{m}{=} \pi(Y).$$

Of course, one might ask whether the reverse implication of Thm. 4 holds, i.e., whether any PTE_d-solution can be obtained from a switching component. While this is certainly true in a weak sense, we remark that stronger notions are currently investigated.

Another obvious question is to ask whether there are PTE_2 solutions for every k. The answer is provided in the next theorem, which is very much in the spirit of the theorem proved by Prouhet (see [197, 242]).

Theorem 6. For every $k \in \mathbb{N}$ there exist PTE_2 solutions for (k, n) with $n = 2^k$.

The proof of this theorem is elementary as it follows directly from Thm. 4 and the standard construction of switching components (see, e.g., [155]). Also Frolov's theorem [80], stated above, follows rather elementary from Thm. 4, since under any non-degenerated affine transformation, a switching component remains a switching component.

Similarly, as for the PTE problem we might ask whether there are ideal solutions to PTE_2. A first answer is given in the following theorem.

Theorem 7. There exist ideal solutions $X \overset{k}{=} Y$ to PTE_2 if $k \in \{1, 2, 3, 5\}$. Infinite solution families are provided in Table 2 (with the conditions on the parameters listed in Table 3).

For a proof it suffices (by Thm. 4) to verify that the sets in Table 2 are indeed $(k+1)$-switching components.

k	X, Y
1	$\{(0,0)^T, (\alpha+\gamma, \beta+\delta)^T\}$, $\{(\alpha,\beta)^T, (\gamma,\delta)^T)\}$
2	$\{(0,0)^T, (\alpha+\beta,\gamma)^T, (2\beta-\alpha, 2\gamma)^T\}$, $\{(\alpha,0)^T, (2\beta, 2\gamma)^T, (\beta-\alpha,\gamma)^T\}$
3	$\{(0,0)^T, (\alpha+\beta,\gamma)^T, (\alpha, 2\gamma+\alpha\gamma/\beta)^T, (-\beta, \gamma+\alpha\gamma/\beta)^T\}$, $\{(\alpha,0)^T, (\alpha+\beta,\gamma+\alpha\gamma/\beta)^T, (0, 2\gamma+\alpha\gamma/\beta)^T, (-\beta,\gamma)^T\}$
5	$\{(0,0)^T, (2\alpha+\beta,\beta)^T, (3\alpha+\beta, 3\alpha+3\beta)^T, (2\alpha, 6\alpha+4\beta)^T, (-\beta, 6\alpha+3\beta)^T, (-\alpha-\beta, 3\alpha+\beta)^T\}$, $\{(2\alpha,0)^T, (3\alpha+\beta, 3\alpha+\beta)^T, (2\alpha+\beta, 6\alpha+3\beta)^T, (0, 6\alpha+4\beta)^T, (-\alpha-\beta, 3\alpha+3\beta)^T, (-\beta,\beta)^T\}$

Table 2: Ideal solutions $X \overset{k}{=} Y$ to PTE_2 for $k \in \{1,2,3,5\}$. The conditions on the parameters $\alpha, \beta, \gamma, \delta \in \mathbb{Z}$ are given in Table 3.

k	Conditions on $\alpha, \beta, \gamma, \delta$
1	$(\alpha,\beta)^T$, $(\gamma,\delta)^T$ pairwise linearly independent (p.l.i.)
2	$(\alpha,0)^T$, $(\beta,\gamma)^T$, $(\beta-\alpha,\gamma)^T$ p.l.i.
3	$(\alpha,0)^T$, $(\beta,\gamma)^T$, $(0,\alpha\gamma/\beta)^T$, $(-\beta,\gamma)^T$ p.l.i., $\alpha,\beta,\gamma > 0$, $\beta \mid \alpha\gamma$
5	$(2\alpha,0)^T$, $(\beta,\beta)^T$, $(\alpha,3\alpha)^T$, $(0,2\beta)^T$, $(-\alpha,3\alpha)^T$, $(-\beta,\beta)^T$ p.l.i., $\alpha,\beta > 0$

Table 3: The conditions on the parameters $\alpha, \beta, \gamma, \delta \in \mathbb{Z}$ from Table 2.

We remarked already that solutions to the $\mathbb{Z}[i]$-PTE problem can be obtained from PTE_2-solutions (via the map $f : \mathbb{Z}^2 \to \mathbb{Z}[i]$, $(\xi_1, \xi_2)^T \mapsto \xi_1 + \xi_2 i$). However, there are also solutions to the $\mathbb{Z}[i]$-PTE problem that do not arise as solutions of the mentioned form. This can be seen, for instance, by considering

$$\{0, 2i, 2+i\} \overset{2}{=} \{i, 1+i, 1+i\}.$$

Our next theorem (a combination of [H12, Lem. 5] and [H12, Thm. 6]) shows that the approach from Thm. 4 cannot yield ideal PTE_2-solutions if $k \in \mathbb{N} \setminus \{1,2,3,5\}$.

Theorem 8. There is no m-switching component (X, Y) in $\mathbb{Z}^2$ with $m \in \mathbb{N}\setminus\{1,2,3,4,6\}$ and $|X| = |Y| = m$.

Our proof is geometric. We first show that the two sets of points of such an m-switching component must be the vertices of a special type of convex lattice polygon (a so-called

lattice $\mathcal{L}$-gon); see [H12, Lem. 5]. It is known from [84, Thm. 4.5] that there are no such $\mathcal{L}$-gons for $m > 6$, and since we separately rule out the case $m = 5$ (see [H12, Thm. 6]) we obtain the claimed result.

We remark that the long-standing open question whether for every k there exist ideal solutions to PTE_1 remains open.

2.1.3 Results from [H9]

With a view towards the results presented in the previous section it seems natural to ask for m-switching components of smallest size.

To make this precise, let $\mathbb{K} \in \{\mathbb{Z}, \mathbb{R}\}$, and let $\psi_{\mathbb{K}^d}(m)$ denote the minimum number n for which there exist m different directions $S_1, \ldots, S_m$ (not all contained in a proper subspace of $\mathbb{R}^d$) such that two different n-point sets in $\mathbb{K}^d$ exist that have the same X-rays in these directions.

In the literature, the exponential bound $\psi_{\mathbb{Z}^d}(m) \leq 2^{m-1}$ has been observed many times. In [H9] we provide the bound

$$\psi_{\mathbb{K}^d}(m) = O(m^{d+1+\varepsilon}), \qquad \varepsilon > 0,$$

which, to our knowledge, is the first polynomial bound for the cases $\mathbb{K}^d = \mathbb{Z}^2$ and $\mathbb{K}^d \in \{\mathbb{Z}^d, \mathbb{R}^d\}$ with $d \geq 3$. (A linear bound for the case $\mathbb{K}^d = \mathbb{R}^2$ follows by considering the switching component obtained by a two-coloring of the vertices of the regular $2m$-gon in $\mathbb{R}^2$.)

The polynomial bound for $\mathbb{K}^d = \mathbb{Z}^2$ implies a polynomial bound for the sizes of solutions to both the classical PTE_1 and the PTE_2 problem. Moreover, we establish a lower bound on $\psi_{\mathbb{Z}^2}$, which enables us to prove a strengthened version of a theorem by Rényi [203] for points in $\mathbb{Z}^2$.

Let us take a closer look.

In [165] Matoušek, Přívětivý, and Škovroň show that there is a number m_0 and a constant $C > 0$ such that for every $m \geq m_0$ almost all (in the sense of measure) sets of m directions allow for a unique reconstruction of any $F \subseteq \mathbb{R}^2$ with $|F| \leq 2^{Cm/\log(m)}$. In other words, for almost all sets of $m \geq m_0$ directions, the smallest size switching components are larger than $2^{Cm/\log(m)}$. Surprisingly, the situation is fundamentally different for carefully selected sets of directions.

Theorem 9. For every $\varepsilon > 0$ and $d \geq 2$ it holds that $\psi_{\mathbb{Z}^d}(m) = O(m^{d+1+\varepsilon})$.

Let us briefly sketch the proof of our result.

Similarly to the proofs of the polynomial size bounds on the classical PTE problem (see [241]) the proof relies on the pigeonhole principle and is hence non-constructive. For given ε and d, we define suitable functions $b_{\varepsilon,d}$, $n_{\varepsilon,d}$, $l_d : \mathbb{N} \to \mathbb{N}$ of the single variable m. For large m, we show that the total number of different $n_{\varepsilon,d}(m)$-point sets in $[b_{\varepsilon,d}(m)]^d$ is larger than the total number of data (i.e., different X-rays) they can generate for some suitable set of m directions $S_1 := \mathrm{lin}(s_1), \ldots, S_m := \mathrm{lin}(s_m)$, with $s_1, \ldots, s_m \in [l_d(m)]^d$. In this case, $[b_{\varepsilon,d}(m)]^d$ must contain two $n_{\varepsilon,d}(m)$-point sets with the same X-rays in directions $s_1, \ldots, s_m$, which proves $\psi_{\mathbb{Z}^d}(m) = O(n_{\varepsilon,d}(m))$. Not only for the asymptotics but also for the pigeonhole principle, it is vital in the proof that there is a suitable balance between the values $b_{\varepsilon,d}(m)$, $n_{\varepsilon,d}(m)$, and $l_d(m)$. It turns out that an appropriate choice of functions $b_{\varepsilon,d}$, $n_{\varepsilon,d}$, and l_d is

$$\begin{aligned} b_{\varepsilon,d}(m) &:= \min\left\{2j \,:\, (j \in \mathbb{N}) \,\wedge\, \left(m^{1+(1+\varepsilon)/d} \leq 2j\right)\right\}, \\ n_{\varepsilon,d}(m) &:= b_{\varepsilon,d}(m)^d/2, \\ l_d(m) &:= \left\lceil \sqrt[d]{2m} \right\rceil. \end{aligned}$$

We remark that in addition to the pigeonhole principle, our proof contains a second non-constructive aspect. In fact, our proof is valid for (almost) every choice of m directions provided that each of the entries of $s_1, \ldots, s_m$ are non-negative and bounded by $l_d(m)$. The existence of such a set of directions is provided by a theorem of Nymann [179], which states that the number $R_d(l_d(m))$ of relatively prime d-tuples in $[l_d(m)]^d$ satisfies

$$\lim_{l_d(m)\to\infty} \frac{R_d(l_d(m))}{l_d(m)^d} = \frac{1}{\zeta(d)},$$

where ζ denotes the *Riemann zeta function*; hence, for large m there exist

$$R_d(l_d(m)) \geq l_d(m)^d/\zeta(2) > l_d(m)^d/2 \geq m,$$

different directions in $[l_d(m)]^d$. This concludes our sketch of the proof of Thm. 9.

Another next natural question is to ask for lower bounds on $\psi_{\mathbb{Z}^d}(m)$. Since $\mathbb{Z}^d \subseteq \mathbb{R}^d$, we clearly have $\psi_{\mathbb{R}^d} \leq \psi_{\mathbb{Z}^d}$, with $\psi_{\mathbb{R}^d}(m)$ denoting the minimum number n for which there exist m different directions $S_1, \ldots, S_m$ (not all contained in a proper subspace of $\mathbb{R}^d$) such that two different n-point sets in $\mathbb{R}^d$ exist that have the same X-rays in these directions.

Rényi's theorem (proved in [203] and generalized to arbitrary dimensions by Heppes [113]), states that any m-point set in $\mathbb{R}^d$ is uniquely determined by its X-rays from $m+1$ different directions. Hence,

Proposition 10 (Rényi, 1952).
For every $d \geq 2$ and $m \in \mathbb{N}$ we have $\psi_{\mathbb{Z}^d}(m) \geq \psi_{\mathbb{R}^d}(m) \geq m$.

The Rényi bound $\psi_{\mathbb{R}^d}(m) \geq m$, for $d = 2$, is tight for all $m \geq 2$. It is also known that the corresponding Rényi bound $\psi_{\mathbb{Z}^2}(m) \geq m$ is tight for $m \in \{1, 2, 3, 4, 6\}$ (see, e.g., examples provided in [86] and [H12]). Interestingly, however, the Rényi bound on $\psi_{\mathbb{Z}^2}(m)$ can be improved (hence showing $\psi_{\mathbb{R}^2} \neq \psi_{\mathbb{Z}^2}$). In [H9] we prove the following result.

Theorem 11. If $m = 5$ or $m > 6$ then $\psi_{\mathbb{Z}^2}(m) \geq m + 1$.

Stated differently, any m-point set in $\mathbb{Z}^2$ with $m = 5$ or $m > 6$ is uniquely determined by its X-rays taken from at least m different directions. The sharpness of this improved Rényi bound for $m = 5$ can be seen from Fig. 2(a). It seems that further improvements on this bound are possible for larger m (see also Sect. 2.1.4).

We remark that the upper bound from Thm. 9 and the two coloring of the vertices of the regular $2m$-gon in $\mathbb{R}^2$ yield the following corollary.

Corollary 12. For every $\varepsilon > 0$ and $d \geq 2$, it holds that

$$\psi_{\mathbb{R}^d}(m) = \begin{cases} m & \text{if} \quad d = 2, \\ O(m^{d+1+\varepsilon}) & \text{if} \quad d > 2. \end{cases}$$

We have now come full circle. The fact that there exist polynomial size switching components (Thm. 9) implies (with Thm. 4) that there exist also polynomial size solution to PTE_2 for every k.

Corollary 13. For every $\varepsilon > 0$ and $k \in \mathbb{N}$ there exists a constant $C > 0$ such that there are solutions

$$\{\xi_1, \ldots, \xi_n\} \stackrel{k}{=} \{\eta_1, \ldots, \eta_n\}$$

of PTE_2 with $n \leq Ck^{3+\varepsilon}$.

This result improves on Thm. 6. However, no constructive method for generating such polynomial size switching components is known.

In the same way as for Cor. 13, we obtain directly from Thm. 9 and Cor. 5 the result that for every $k \in \mathbb{N}$, there exist PTE_1-solutions for (k, n) with $n = O(k^{3+\varepsilon})$, $\varepsilon > 0$. Better bounds (quadratic in k) can be obtained by applying the pigeonhole principle directly to the PTE_1-problem (see the remarkably short proof by Wright [241]). No constructive method is known that provides polynomial size PTE_1-solutions.

2.1.4 Additional Comments On Switching Components

Switching components seem to appear first in the work of Ryser [210]. Later work on switching components includes [46, 108, 130, 141, 165, 218]. Computational

investigations related to the explicit construction of switching components can be found in [41, 226, 227, 228, 247]. We remark that the papers [226, 227, 228] deal with the so-called *finite Radon transform* where the projection lines wrap whenever they encounter any boundary of the image, the paper [247] deals with compositions of switching components for generalized projections, and in the paper [41] the task of generating small switching components that fit into a small rectangle is studied. The first computational study on generating minimal switching components seems to have been performed by Kiermaier [134].

It is an interesting open question to determine the precise values of $\psi_{\mathbb{Z}^d}(m)$, even for small m. Figure 2 shows examples of small switching components in $\mathbb{Z}^2$ for $m \in \{6, \ldots, 10\}$ (the computational search by Kiermaier [134] provided different examples of the same size. Of course, the examples yield upper bounds on the respective values of $\psi_{\mathbb{Z}^2}(m)$. Lower bounds are provided by Thms. 10 and 11. In Table 4 the values of $\psi_{\mathbb{Z}^2}(m)$ are shown for $m \in [10]$ (the pairs provided for $m \geq 7$ show the currently best lower and upper bound on $\psi_{\mathbb{Z}^2}(m)$).

m	1	2	3	4	5	6	7	8	9	10
$\psi_{\mathbb{Z}^2}(m)$	1	2	3	4	6	6	$(8, 10)$	$(9, 12)$	$(10, 18)$	$(11, 20)$

Table 4: Values of $\psi_{\mathbb{Z}^2}(m)$ for $m \in [10]$. In the cases $m \geq 7$, the pair of currently best lower and upper bounds on $\psi_{\mathbb{Z}^2}(m)$ is shown.

2.1.5 Results from [H5]

In [H5] we consider questions of *stability*, *error correction*, and *noise compensation* in *discrete tomography*.

Discrete tomography deals with the reconstruction of finite sets from knowledge about their interaction with certain query sets. The most prominent example is that of the reconstruction of a finite subset F of $\mathbb{Z}^d$ from its X-rays (i.e., line sums) in a small positive integer number m of directions. Applications of discrete tomography include particle tracking in plasma physics, quality control in semiconductor industry, image processing, graph theory, scheduling, statistical data security, game theory, etc. (see, e.g., [H7, H14, 77, 85, 86, 100, 101, 115, 116, 121, 210, 221]). The reconstruction task is an *ill-posed* discrete inverse problem, depicting (suitable variants of) all three Hadamard criteria [106] for ill-posedness. In fact, for general data there need not exist a solution, if the data is consistent, the solutions need not be uniquely determined, and even in the case of uniqueness, the solution may change dramatically with small changes of the data [8, 13].

In our paper [H5] we address in particular the following problems. Does discrete tomography have the power of *error correction*? Can noise be compensated by taking more X-ray images, and if so, what is the quantitative effect of taking one more X-ray?

A key argument that we employ in this paper is the fact that there exist no PTE solutions for (k, n) if $n \leq k$.

In the following, let $d, m \in \mathbb{N}$ with $d \geq 2$. We use the same notation as in Sect. 2.1.1. In particular, we have again $\mathbb{K}^d \in \{\mathbb{R}^d, \mathbb{Z}^d\}$.

Given m different lines $S_1, \ldots, S_m \in \mathcal{S}^d$, the basic questions in discrete tomography are as follows. What kind of information about a finite (lattice) set $F \in \mathbb{K}^d$ can be retrieved from its X-ray images $X_{S_1}F, \ldots, X_{S_m}F$? How difficult is the reconstruction algorithmically? How sensitive is the task to data errors? Here the data are given in terms of functions

$$f_j : \mathcal{A}_{\mathbb{K}}(S_j) \to \mathbb{N}_0, \qquad j \in [m]$$

with finite support $\mathcal{T}_j \subseteq \mathcal{A}_{\mathbb{K}}(S_j)$ represented by appropriately chosen data structures; see [86]. Hence the difference of two data functions with respect to the same line $S \in \mathcal{S}^d$ is a function $h : \mathcal{A}_{\mathbb{K}}(S) \to \mathbb{Z}$; its size will be measured in terms of its ℓ_1-*norm*

$$\|h\|_1 = \sum_{T \in \mathcal{A}_{\mathbb{K}}(S)} |h(T)|.$$

Our main stability result from [H5] is as follows.

Theorem 14. Let $S_1, \ldots, S_m \in \mathcal{S}^d$ be different and $F_1, F_2 \in \mathcal{F}^d(\mathbb{K})$ with $|F_1| = |F_2|$. If

$$\sum_{j=1}^{m} ||X_{S_j}F_1 - X_{S_j}F_2||_1 < 2(m-1)$$

then F_1 and F_2 are tomographically equivalent.

This stability result is best possible since we have shown in [8] (see also [11, 13]) that there exist arbitrarily large lattice sets F_1, F_2, even of the same cardinality and uniquely determined by their respective X-rays, which satisfy $\sum_{j=1}^{m} ||X_{S_j}F_1 - X_{S_j}F_2||_1 = 2(m-1)$, but which are disjoint or, even more generally, "dissimilar" under affine transformations. (Further stability results for the particular case $m = 2$ can be found in [9, 10, 57].)

Theorem 14 is equivalent to

Theorem 15. Let $S_1, \ldots, S_m \in \mathcal{S}^d$ be different. Then there are no $F_1, F_2 \in \mathcal{F}^d(\mathbb{K})$ with $|F_1| = |F_2|$ and $0 < \sum_{j=1}^{m} ||X_{S_j}F_1 - X_{S_j}F_2||_1 < 2(m-1)$.

The proof of this theorem relies on a combination of some combinatorial, geometric, and algebraic arguments. One key algebraic argument is the restatement of the fact that there exist no PTE solutions for $(k, n) = (m-2, m-2)$. A short proof of this fact can be given by using the *Newton identities* (for the identities see, e.g., [172]).

As direct corollaries to Thm. 14, it is possible to derive "noisy versions" of known uniqueness theorems. The two following examples are given in our paper.

Recall from Sect. 2.1.1 that Rényi's theorem [203] states that if we know the cardinality $|F|$ of a finite set F we can guarantee uniqueness from X-rays taken in any $m \geq |F|+1$ different directions. Our first corollary shows that we can guarantee uniqueness, *even if the X-rays are not given precisely.*

Corollary 16. Let $F_1, F_2 \in \mathcal{F}^d(\mathbb{K})$ with $|F_1| = |F_2|$, $m \in \mathbb{N}$ with $m \geq |F_1| + 1$, and let $S_1, \ldots, S_m \in \mathcal{S}^d$ be different. If $\sum_{j=1}^m ||X_{S_j} F_1 - X_{S_j} F_2||_1 < 2|F_1|$, then $F_1 = F_2$.

In fact, this corollary shows the potential power of error correction in the setting of Rényi's theorem: A total error smaller than $2|F|$ can be compensated without increasing the number of X-rays taken if the cardinality $|F|$ of the original set F is known. But even without knowing $|F|$ precisely we can correct errors at the expense, however, of taking more X-rays.

Corollary 17. Let $F_1, F_2 \in \mathcal{F}^d(\mathbb{K})$ with $|F_1| \leq |F_2|$, $m \in \mathbb{N}$ with $m \geq 2|F_1|$, and let $S_1, \ldots, S_m \in \mathcal{S}^d$ be different. Then $\sum_{j=1}^m ||X_{S_j} F_1 - X_{S_j} F_2||_1 < 2|F_1|$ implies $F_1 = F_2$.

Our next example gives a stable version of a theorem of Gardner and Gritzmann [84] for the set $\mathcal{C}^d$ of *convex lattice sets*, i.e., of sets $F \in \mathcal{F}^d$ with $F = \mathrm{conv}(F \cap \mathbb{Z}^d)$.

Corollary 18. Let F_1, $F_2 \in \mathcal{C}^d$ with $|F_1| = |F_2|$.

(i) There are sets $\{S_1, S_2, S_3, S_4\} \subseteq \mathcal{L}^d$ of four lines such that $\sum_{j=1}^4 ||X_{S_j} F_1 - X_{S_j} F_2||_1 < 6$ implies $F_1 = F_2$.

(ii) For any set $\{S_1, \ldots, S_m\} \subseteq \mathcal{L}^d$ of $m \geq 7$ coplanar lattice lines, $\sum_{j=1}^m ||X_{S_j} F_1 - X_{S_j} F_2||_1 < 2(m-1)$ implies $F_1 = F_2$.

We then turn to results on some algorithmic tasks related to questions of stability in discrete tomography. We concentrate on the case of finite lattice sets whose X-rays are taken in lattice directions. So, let $S_1, \ldots, S_m \in \mathcal{L}^d$.

As algorithmic consequences of Thm. 14, we can give "noisy extensions" of known complexity results. For instance, it is known that the two problems

CONSISTENCY$_{\mathcal{F}^d}(S_1, \ldots, S_m)$
Input: For $j \in [m]$ data functions $f_j : \mathcal{A}_{\mathbb{Z}}(S_j) \to \mathbb{N}_0$ with finite support.
Question: Does there exist a finite lattice set $F \in \mathcal{F}^d$ such that $X_{S_j} F = f_j$ for $j \in [m]$?

and

UNIQUENESS$_{\mathcal{F}^d}(S_1, \ldots, S_m)$
Input: A set $F_1 \in \mathcal{F}^d$.
Question: Does there exist a set $F_2 \in \mathcal{F}^d$ with $F_1 \neq F_2$ such that $X_{S_j} F_1 = X_{S_j} F_2$ for $j \in [m]$?

can be solved in polynomial time for $m \leq 2$ but are $\mathbb{NP}$-complete for $m \geq 3$ (see [86]). Theorem 14 (in combination with several technical lemmas) allows us to extend these results as follows.

Corollary 19. Let $S_1, \ldots, S_m \in \mathcal{L}^d$ be different. The following two problems

X-RAY-CORRECTION$_{\mathcal{F}^d}(S_1, \ldots, S_m)$
Input: For every $j \in [m]$ a data function $f_j : \mathcal{A}_{\mathbb{Z}}(S_j) \to \mathbb{N}_0$ with finite support.
Question: Does there exist a finite lattice set $F \in \mathcal{F}^d$ with $\sum_{j=1}^m ||X_{S_j} F - f_j||_1 \leq m - 1$?

and

SIMILAR-SOLUTION$_{\mathcal{F}^d}(S_1, \ldots, S_m)$SIMILAR-SOLUTION$_{\mathcal{F}^d}(S_1, \ldots, S_m)$
Input: A finite lattice set $F_1 \in \mathcal{F}^d$
Question: Does there exist a finite lattice set $F_2 \in \mathcal{F}^d$ with $|F_1| = |F_2|$ and $F_1 \neq F_2$ such that $\sum_{j=1}^m ||X_{S_j} F_1 - X_{S_j} F_2||_1 \leq 2m - 3$?

are in $\mathbb{P}$ for $m \leq 2$ but are $\mathbb{NP}$-complete for $m \geq 3$.

Note that X-RAY-CORRECTION$_{\mathcal{F}}(S_1, \ldots, S_m)$ can also be formulated as the task to decide for given data functions $f_j : \mathcal{A}_{\mathbb{Z}}(S_j) \to \mathbb{N}_0$, $j \in [m]$, with finite support, whether there exist "corrected" data functions $g_j : \mathcal{A}_{\mathbb{Z}^d}(S_j) \to \mathbb{N}_0$, $j \in [m]$, with finite support that are consistent and do not differ from the given functions by more than a total of $m - 1$. Corollary 19 shows that this form of measurement correction is just as hard as checking consistency.

If the data is noisy it seems natural to try to find a finite lattice set that fits the measurements best. This task is discussed in the following theorem from our paper.

Theorem 20. Let $S_1, \ldots, S_m \in \mathcal{L}^d$ be different. The problem

NEAREST-SOLUTION$_{\mathcal{F}^d}(S_1, \ldots, S_m)$
Input: For every $j \in [m]$, data functions $f_j : \mathcal{A}_{\mathbb{Z}}(S_j) \to \mathbb{N}_0$ with finite support.
Task: Determine a set $F^* \in \mathcal{F}^d$ such that $\sum_{j=1}^m ||X_{S_j} F^* - f_j||_1 = \min_{F \in \mathcal{F}^d} \sum_{j=1}^m ||X_{S_j} F - f_j||_1$,

is in $\mathbb{P}$ for $m \leq 2$ but is $\mathbb{NP}$-hard for $m \geq 3$.

The $\mathbb{NP}$-hardness result for $m \geq 3$ follows rather directly from known complexity results. The proof of the polynomial-time solvability in the case $m = 2$ is more involved (ultimately, the problem is reduced to a linear programming problem involving a totally unimodular matrix).

3 Tomographic Super-Resolution Imaging, [H4]

3.1 Algorithms and Complexity

Different imaging techniques in tomography have different characteristics that strongly depend on the specific data acquisition setup and the imaged tissue/material. It is a major issue (and at the heart of current research, see, e.g., [27, 60, 119, 160, 164, 186, 212]) to improve the resolution of an image by combining different imaging techniques.

3.1.1 Results from [H4]

Our results in [H4] are motivated by the task of enhancing the resolution of reconstructed tomographic images obtained from binary objects representing, for instance, crystalline structures, nanoparticles or two-phase samples [H2, H7, H14, 215, 233].

We study the task of reconstructing binary $m \times n$-images from row and column sums and additional constraints, so-called *block constraints*, on the number of black pixels to be contained in the $k \times k$-blocks resulting from a subdivision of each pixel in the $m/k \times n/k$ low-resolution image. Figure 3 illustrates the process.

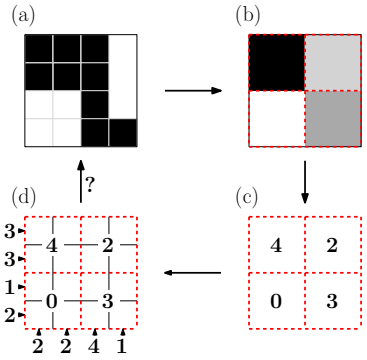

Figure 3: The double-resolution imaging task DR. (a) Original (unknown) high-resolution image, (b) the corresponding low-resolution grayscale image, (c) gray levels converted into block constraints, (d) taken in combination with double-resolution row and column sum data. The task is to reconstruct from (d) the original binary image shown in (a).

Going into some more details, we introduce some notation. We call any set $([a,b] \times [c,d]) \cap \mathbb{Z}^2$, with $a,b,c,d \in \mathbb{Z}$ and $a \le b$, $c \le d$, a *box*. For $j_1, j_2 \in \mathbb{N}$, we set $B_k(j_1,j_2) := B(j_1,j_2) := (j_1,j_2) + [k-1]_0^2$. Defining for any $k \in \mathbb{N}$ and $m,n \in k\mathbb{N}$ the set of *(lower-left) corner points* $C(m,n,k) := ([m] \times [n]) \cap (k\mathbb{N}_0 + 1)^2$, we call any box $B_k(j_1,j_2)$ with $(j_1,j_2) \in C(m,n,k)$ a *block*. The blocks form a partition of $[m] \times [n]$, i.e., $\dot{\bigcup}_{(j_1,j_2)\in C(m,n,k)} B_k(j_1,j_2) = [m] \times [n]$.

For $\varepsilon, k \in \mathbb{N}_0$ with $k \ge 2$ the task of *(noisy) super-resolution* is the following.

nSR(k,ε)

Instance: $m,n \in k\mathbb{N}$,

$r_1,\dots,r_n \in \mathbb{N}_0$, (row sum measurements)

$c_1,\dots,c_m \in \mathbb{N}_0$, (column sum measurem.)

$R \subseteq C(m,n,k)$, (corner points of reliable gray value measurem.)

$v(j_1,j_2) \in [k^2]_0$, $(j_1,j_2) \in C(m,n,k)$, (gray value measurem.)

Task: Find $\xi_{p,q} \in \{0,1\}$, $(p,q) \in [m] \times [n]$, with

$$\sum_{p\in[m]} \xi_{p,q} = r_q, \quad q \in [n], \quad \text{(row sums)}$$

$$\sum_{q\in[n]} \xi_{p,q} = c_p, \quad p \in [m], \quad \text{(column sums)}$$

$$\sum_{(p,q)\in B_k(j_1,j_2)} \xi_{p,q} = v(j_1,j_2), \quad (j_1,j_2) \in R, \quad \text{(block constraints)}$$

$$\sum_{(p,q)\in B_k(j_1,j_2)} \xi_{p,q} \in v(j_1,j_2) + [-\varepsilon,\varepsilon], \quad (j_1,j_2) \in C(m,n,k) \setminus R, \quad \text{(noisy block constraints)}$$

or decide that no such solution exists.

The numbers $r_1,\dots,r_n$ and $c_1,\dots,c_m$ are the row and column sum measurements of the higher-resolution binary $m \times n$ image, $v(j_1,j_2) \in [k^2]_0$ corresponds to the gray value of the low-resolution $k \times k$-pixel at (j_1,j_2) of the low-resolution $m/k \times n/k$ grayscale image, and R is the set of low-resolution pixel locations for which we assume that the gray values have been determined reliably, i.e., without error. The number ε is an error bound for the remaining blocks. The task is to find a binary high-resolution image satisfying the row and column sums such that the number of black pixels in each block adds up to a gray value for the corresponding $k \times k$-pixel in the lower-resolution image that lies in the specified interval.

Our special focus in [H4] is on double-resolution imaging, i.e., on the case $k = 2$.

For $\varepsilon > 0$, let $\text{NDR}(\varepsilon) = \text{NSR}(2, \varepsilon)$. In the reliable situation, i.e., for $\varepsilon = 0$, we simply speak of *double-resolution* and set $\text{DR} = \text{NSR}(2, 0)$.

Our first result in [H4] is the following.

Theorem 21. $\text{DR} \in \mathbb{P}$.

The proof of this theorem (relying on four lemmas and a corollary) can be briefly sketched as follows.

The main step in the proof of Thm. 21 is to show that DR decomposes into five problems $\text{DR}(\nu)$, $\nu \in [4]_0$, each of which can be solved independently. This decomposition property of DR is proved by combinatorial reasoning, introducing the concept of *local switches* (which are special *interchanges* in the sense of [210]) and the notion of *reduced solutions*. In fact, we show that if an instance of DR has a solution, then there is also a reduced solution, and the reduced solution can be found by solving suitable instances of the problems $\text{DR}(\nu)$, $\nu \in [4]_0$.

The problems $\text{DR}(\nu)$, $\nu \in [4]_0$, are single-graylevel versions of DR where each non-empty block is required to contain the same number ν of ones. It is easy to see that, DR(0) and DR(4) can be solved in polynomial-time. In seperate lemmas we prove that also DR(1), DR(2), and DR(3) are polynomial-time solvable.

Based on the decomposition of DR into the subproblems, we show the following.

Theorem 22. For every instance of DR it can be decided in polynomial time whether the instance admits a unique solution.

We then turn to the task $n\text{DR}(\varepsilon)$ where small "occasional" uncertainties in the gray levels are allowed.

Theorem 23. $\text{NDR}(\varepsilon)$ is $\mathbb{NP}$-hard for any $\varepsilon > 0$.

The problem remains $\mathbb{NP}$-hard for larger block sizes.

Corollary 24. $\text{NSR}(k, \varepsilon)$ is $\mathbb{NP}$-hard for any $k \geq 2$ and $\varepsilon > 0$.

In the proof of Thm. 23 (and Cor. 24) we use a transformation from the $\mathbb{NP}$-hard problem 1-IN-3-SAT (see [54]), which asks for a satisfying truth assignment that sets exactly one literal TRUE in each clause of a given Boolean formula in conjunctive normal form where all clauses contain three literals (involving three different variables).

We remark that our complexity results can also be interpreted in the context of discrete tomography. In discrete tomography it is well known that the problem of reconstructing binary images from X-ray data taken from two directions can be solved in polynomial

time [81, 210]. Typically, this information does not determine the image uniquely (see, e.g., [102] and the papers quoted therein). Hence, one would like to take and utilize additional measurements. If, however, additional constraints are added that enforce that the solutions satisfy the X-ray data taken from a third direction, then the problem becomes $\mathbb{NP}$-hard, and it remains $\mathbb{NP}$-hard if X-ray data from even more directions are given [86] (see also [66] for results on a polyatomic version).

The case of block constraints behaves somewhat differently. Theorem 23 and Cor. 24 show that the problem of reconstructing a binary image from X-ray data taken from two directions is again $\mathbb{NP}$-hard if *several* (but not all) block constraints (which need to be satisfied with equality) are added. However, and possibly less expectedly, if *all* block constraints are included, then the problem becomes polynomial-time solvable (Thm. 21). If, on the other hand, from *all* block constraints *some* of the data comes with *noise* at most ± 1, then the problem becomes again $\mathbb{NP}$-hard (Thm. 23 and Cor. 24). And yet again, if from *all* block constraints *all* of the data is *sufficiently noisy*, then the problem is in $\mathbb{P}$ (as this is again the problem of reconstructing binary images from X-ray data taken from two directions). See Fig. 4 for an overview of these complexity jumps.

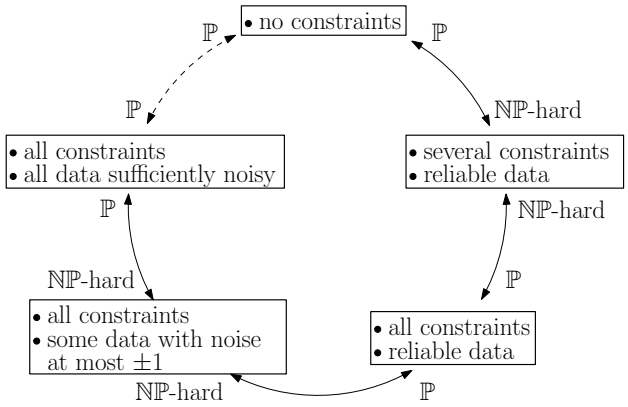

Figure 4: Overview of complexity jumps for the problem of reconstructing a binary image from row and column sums and additional block constraints.

4 Tomographic Point Tracking: Theory and Applications, [H3, H6, H7, H14]

4.1 Theory

We consider the problem of determining the paths $\mathcal{P}_1, \ldots, \mathcal{P}_n$ of n points in space over a period of $t \in \mathbb{N}$ moments in time from X-ray images taken from a fixed number m of directions. We refer to this problem, lying at the heart of *dynamic discrete tomography*, as *tomographic point tracking*. (For an artistic illustration see our DFG calender image [12].) As it turns out, the problem comprises two different but coupled basic underlying tasks, the reconstruction of a finite set of points from few of their X-ray images (*discrete tomography*) and the identification of the points over time (*tracking*).

4.1.1 Results from [H3]

In [H3], we study the tomographic tracking problem from a mathematical and algorithmic point of view with a special focus on the interplay between discrete tomography and tracking. Therefore we distinguish the cases that for none, some or all of the t moments $\tau_1, \ldots, \tau_t$ in time, a solution of the discrete tomography task at time $\tau_1, \ldots, \tau_t$ is explicitly available. We refer to the first case as the *positionally determined* case while, in the more general situation, we speak of the *(partially)* or *(totally) tomographic* case of point tracking.

By modeling the problem as $t-1$ uncoupled *minimum weight perfect bipartite matching* problems, we show for the positionally determined case that the tracking problem can be solved in polynomial time if the problem exhibits a certain *Markov-type property* (which, effectively, allows only dependencies between any two consecutive time steps).

The partially tomographic case even for $t = 2$, however, is $\mathbb{NP}$-hard. We show this by using a reduction from $\textsc{Consistency}_{\mathcal{F}^d}(S_1, S_2, S_3)$; see Sect. 2.1.5. Complementing this result, we consider the tomographic tracking problem for two directions where the so-called *displacement field* is assumed to be given (the displacement field uniquely determines the points's next position). Again, this problem turns out to be $\mathbb{NP}$-hard already for $t = 2$ and rather general classes of displacement fields.

We then turn to the rolling horizon approach that we will describe in Sect. 4.1.3. First, we give an example that shows that this approach does not always yield the correct solution. Then, we study the issue of of how to incorporate additional prior knowledge of the point history into the models. We show, under rather general assumptions, that already in the positionally determined case the tracking problems becomes $\mathbb{NP}$-hard for $t > 2$. In particular, by making use of a result of [224] on a

variant of 3D-Matching [129], we show that even if the points are known to move along straight lines, this prior knowledge cannot efficiently be exploited algorithmically (unless $\mathbb{P} = \mathbb{NP}$).

We proceed by introducing three algorithms that can be viewed as rather general paradigms of heuristics that involve prior knowledge about the movement of the points and which can be used in the tomographic case.

We then discuss *combinatorial models* (see also the next subsection and Sect. 3). In these models the positions of the points in the next time step are assumed to be known approximatively in the sense that the candidate positions are confined to certain *windows*, which are finite subsets of positions. Again, under rather general conditions, we show $\mathbb{NP}$-hardness of the respective tomographic tracking tasks. However, we also identify polynomial-time solvable special cases of practical relevance.

4.1.2 Results from [H6]

In [H6] we study several classes of the above mentioned *combinatorial models*. In particular, we study the computational complexity of the *discrete inverse problem* of reconstructing binary matrices from their row and column sums under additional constraints on the number and pattern of entries in specified minors. We focus on special types of *windows*, called *blocks of size* k, which are sets $I_1 \times I_2$ with I_1 and I_2, respectively, denoting set of k consecutive row and column indices of the binary matrix (see also Sect. 3).

We study the effect of three different parameters: k corresponds to the *size of the block*, ν is the *number of 1's* in the nonzero minors, and a specifies the allowed positions of 1's in the blocks, referred to as the *pattern of the block*. The choice for these parameters will specify the given problem $\textsc{Rec}(k, \nu, a)$, which we will formally introduce further below. Hence k, ν, and a are given beforehand (i.e., they are not part of the input).

We show in [H6] that there are various unexpected complexity jumps back and forth from polynomial-time solvability to $\mathbb{NP}$-hardness. Omitting technical details some of these jumps can be summarized as follows; see Table 5.

For $k = 1$ the problems are in $\mathbb{P}$ regardless on how the other parameters are set; see Thm. 25(i). For $k \geq 2$ it depends on ν and a whether the problems are in $\mathbb{P}$ or $\mathbb{NP}$-hard; see Thms. 25(ii),(iii) and 26. For $k \geq 2$, some values of ν render the problems tractable while others make them $\mathbb{NP}$-hard; see Thms. 25(ii) and 26(ii) even if the patterns are not restricted at all. Adding a pattern constraint may turn an otherwise $\mathbb{NP}$-hard problem into a polynomial time solvable problem; see Thms. 26(ii) and 25(iii). The reverse complexity jump, however, can also be observed; see Thms. 25(ii) and 26(i).

We are now going a bit more into detail (for notation, see also Sect. 3). We introduce

	$\mathbb{P}$	$\mathbb{NP}$-hard
varying k	$\textsc{Rec}(1,2,0)$	$\textsc{Rec}(k,2,0)$
	$\textsc{Rec}(1,1,1)$	$\textsc{Rec}(k,1,1)$
varying ν	$\textsc{Rec}(k,1,0)$,	$\textsc{Rec}(k,2,0)$
varying a	$\textsc{Rec}(k,2,2)$	$\textsc{Rec}(k,2,0)$
	$\textsc{Rec}(k,1,0)$	$\textsc{Rec}(k,1,1)$

Table 5: Computational complexity of $\textsc{Rec}(1,\nu,a)$ and $\textsc{Rec}(k,\nu,a)$ for $k \geq 2$ under change of a single parameter.

three patterns that we study in detail since they exhibit already the general complexity jump behavior we are particular interested in.

The first pattern $P(k,0)$ is unconstrained, i.e., does not pose any additional restrictions on the positions of 1's. The second pattern $P(k,1)$ forces all elements in the $k \times k$ block to be 0 except possibly for the two entries in the lower-left and upper-right corner. The third pattern $P(k,2)$ excludes all patterns that admit more than one 1 in each row of the $k \times k$ block. Here are the formal definitions.

For $k \in \mathbb{N}$ let $2^{[k-1]_0^2}$ denote the power set of $[k-1]_0^2$. Then we set

$$\begin{aligned}
P(k,0) &:= 2^{[k-1]_0^2},\\
P(k,1) &:= \{\{(0,0)\},\{(k-1,k-1)\}\},\\
P(k,2) &:= \{M \in 2^{[k-1]_0^2} \,:\, |M \cap ([k-1]_0 \times \{j\})\,| \leq 1 \text{ for all } j \in [k]_0.\}
\end{aligned}$$

Further, for $(j_1,j_2) \in C(m,n,2)$ and $x = (\xi_{j_1,j_2})_{j_1 \in [m], j_2 \in [n]}$ we set

$$\mathrm{pat}_k(x,j_1,j_2) := \{(p,q) \in B_k(j_1,j_2) \,:\, \xi_{p,q} \neq 0\} - (j_1,j_2).$$

For $k,\nu \in \mathbb{N}$ and $a \in \{0,1,2\}$ we define now the following problem $\textsc{Rec}(k,\nu,a)$.

$\textsc{Rec}(k, \nu, a)$

Instance:	$m, n \in k\mathbb{N}$,		
	$r_1, \ldots, r_n \in \mathbb{N}_0$,		(row sum measurements)
	$c_1, \ldots, c_m \in \mathbb{N}_0$,		(column sum measurements)
	$v(j_1, j_2) \in \{0, \nu\}$,	$(j_1, j_2) \in C(m, n, k)$,	(block measurements)
Task:	Find $\xi_{p,q} \in \{0, 1\}$, $(p, q) \in [m] \times [n]$, with		
	$\sum_{p \in [m]} \xi_{p,q} = r_q$,	$q \in [n]$,	(row sums)
	$\sum_{q \in [n]} \xi_{p,q} = c_p$,	$p \in [m]$,	(column sums)
	$\sum_{(p,q) \in B_k(j_1,j_2)} \xi_{p,q} \leq v(j_1, j_2)$,	$(j_1, j_2) \in C(m, n, k)$,	(block constraints)
	$\mathrm{pat}_k(x, j_1, j_2) \in P(k, a)$,	$(j_1, j_2) \in C(m, n, k)$,	(pattern constraints),
	or decide that no such solution exists.		

In other words, we ask for 0/1-solutions that satisfy given row and column sums, *block constraints* of the form $\sum_{(p,q) \in B_k(j_1,j_2)} \xi_{j_1,j_2} \leq v(j_1, j_2)$ with given $v(j_1, j_2) \in \{0, \nu\}$, and *pattern constraints* that restrict the potential locations of the 1's in each block.

Our main results show that the computational complexity of $\textsc{Rec}(k, \nu, a)$ may change drastically when k, ν, or a is varied.

Theorem 25.

(i) $\textsc{Rec}(1, \nu, a) \in \mathbb{P}$ for any $\nu \in \mathbb{N}$ and $a \in \{0, 1, 2\}$.

(ii) $\textsc{Rec}(k, 1, 0) \in \mathbb{P}$ for any $k \geq 2$.

(iii) $\textsc{Rec}(k, \nu, 2) \in \mathbb{P}$ for any $k \geq 2$ and $\nu \geq k$.

Theorem 26.

(i) $\textsc{Rec}(k, 1, 1) \in \mathbb{NP}$-hard for any $k \geq 2$.

(ii) $\textsc{Rec}(k, 2, 0) \in \mathbb{NP}$-hard for any $k \geq 2$.

The most notable changes are summarized in Table 5. Some of these changes may at first glance seem somewhat counterintuitive. For instance, restricting the solution space via pattern constraints turns the $\mathbb{NP}$-hard problem $\textsc{Rec}(k, 2, 0)$ $(k \geq 2)$, into the polynomial time solvable problem $\textsc{Rec}(k, 2, 2)$. Conversely, additional pattern constraints convert the tractable problem $\textsc{Rec}(k, 1, 0)$ into the $\mathbb{NP}$-hard problem $\textsc{Rec}(k, 1, 1)$ $(k \geq 2)$.

The general ideas behind the proofs of Thms. 25 and 26 can be briefly sketched as follows.

Theorem 25(i) follows directly from known results on the reconstruction from row and column sums where some of the solution values have prescribed values. On the other hand, the proof of Thm. 25(ii) proceeds in two steps. First, a lower-resolution reconstruction from row and column sums is performed, which, in a second step, is extend to full resolution. The proof of Thm. 25(iii) is more involved than the other two proofs. Here, the reconstruction problem is again reduced to the task of solving a linear programming problem involving a *totally unimodular* coefficient matrix. Our proof of the total unimodularity property requires careful counting arguments, which are given in a separate lemma (and which might be of independent interest).

For the intractability results we remark that in the proof of Thm. 26(i) we reduce from the $\mathbb{NP}$-hard problem *3*-COLOR TOMOGRAPHY (see [66]). The proof of Thm. 26(ii) is more involved as we modify the construction used to establish the $\mathbb{NP}$-hardness of NDR(ε), $\varepsilon > 0$.

4.1.3 Results from [H7]

In [H7] we consider the task of tomographic point tracking with a special focus on *particle tracking velocimetry (PTV)*, which is a diagnostic technique that plays an important role in studying flows (see, e.g., [4, 133]) including combustion (see, e.g., [204, 244]). It has also been used to study plasma (see, e.g., [107, 143]). In PTV the motion of particles is followed in a sequence of images for the purpose of measuring their velocities. In complex plasmas the particles themselves are the subject of interest [96, 182] whereas in fluids the particle velocities are nearly the same as the local flow velocities which can hence be studied by PTV. Particle tracking velocimetry is particularly advantageous if the density of particles is intrinsically low or has to be limited.

Previous tomographic particle tracking methods are based on the *multiplicative algebraic reconstruction technique (MART)* [117] and its variants [189, 238]. These are methods for reconstructing the distribution of multiple-pixel sized particles modeled as graylevel images (for a recent approach of reconstructing single-pixel sized particles modeled as graylevel images, see [58]). The graylevel can take any value and is a continuous quantity. The subsequent binarization is usually performed by comparison of the graylevel to a threshold. This procedure is not guaranteed to yield solutions that are consistent with the data. We develop an algorithm that returns *binary solutions* that are consistent with the data as this is explicitly included as a constraint in the imaging model. Information from previously reconstructed frames is incorporated in the reconstruction procedure that is formulated as a discrete optimization problem. It seems that no such methods have previously been developed for PTV.

In [H7] we remark that, in general, PTV may track particle paths that do not exist but which are consistent with the data. Fig. 5 gives an illustration for the case where tomographic data has been obtained from two directions.

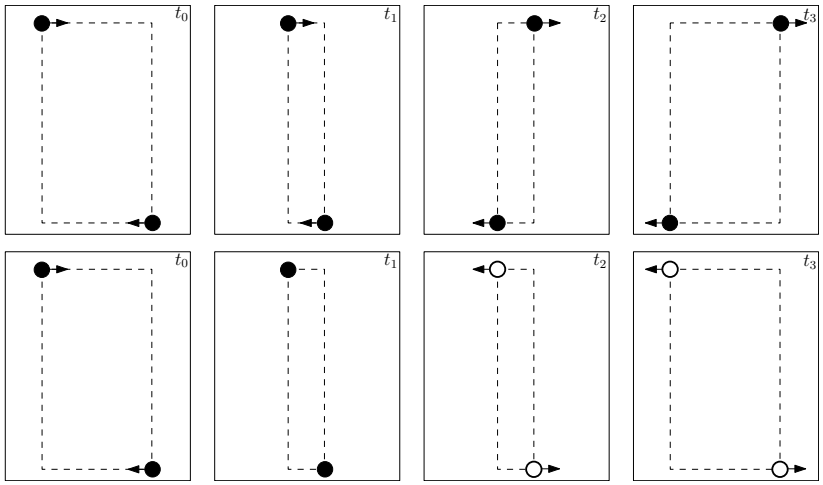

Figure 5: An example illustrating that PTV may track particle paths that do not exist but which are consistent with the data. The upper row shows the movement of two particles in 2D, the second row shows alternative movement, also consistent with the data.

Hence, in our approach we want to be able to incorporate prior knowledge about the possible movement of the particles.

Our approach is a *rolling horizon approach* for tomographic point tracking. For m projection directions (typically orthogonal to the detector plane), m (projecting) lines pass through every particle. The intersections of these projecting lines for every projection direction are called *candidate points*. The set of candidate points is the so-called *candidate grid*; it contains the set of all particle positions and typically, in 2D, many additional points that are all other intersections of these projecting lines. (Generically, the situation is different in 3D since there any two affine lines in general position are disjoint. There are no such additional points in these cases, and therefore the positionally determined case of tomographic point tracking becomes relevant in 3D; see Sect. 4.1.1.)

We consider the reconstruction problem at time t. To each point $g_j^{(t)}$ of the candidate grid $G^{(t)}$ containing $l(t)$ points we associate a variable $\xi_j^{(t)}$. Presence or absence of a particle at $g_j^{(t)}$ is indicated by the value $\xi_j^{*(t)} = 1$ and $\xi_j^{*(t)} = 0$, respectively. The requirement that any solution $x^{*(t)} := (\xi_1^{*(t)}, \ldots, \xi_{l(t)}^{*\ (t)})^T \in \{0,1\}^{l(t)}$ obtained by a

reconstruction algorithm should be consistent with the projection data can be described by a 0-1-system of linear inequalities:

$$A^{(t)}x^{(t)} \geq b^{(t)}, \quad x^{(t)} \in \{0,1\}^{l(t)}, \tag{4}$$

where $b^{(t)} := (1,\ldots,1)^T$ represents the data; $k(t)$ denotes the total number of measurements, and $A^{(t)} \in \{0,1\}^{k(t)\times l(t)}$ collects the individual variables' contributions to the signal as specified by the acquisition geometry. (The '$\geq$' is used in (4) to account for the fact that for projections we cannot distinguish whether one or multiple particles have been detected. In situations where this can be distinguished the '$\geq$' can be replaced by '=,' and the same framework as we will described can be applied.)

For the tracking problem, we need to solve (4) for subsequent time steps and need to be able to match the particles from $x^{*(t-1)}$ to the particles from the $x^{*(t)}$ solution.

Let $w^{(t)} = (\omega_1^{(t-1,t)},\ldots,\omega_{l(t)}^{(t-1,t)})^T \in \mathbb{R}^{l(t)}$ denote a vector specifying weights associated to each candidate grid point (possible choices are discussed below). We introduce the following *discrete optimization problem* for the tracking step from $t-1 \to t$:

$$\begin{aligned} \min \quad & {w^{(t)}}^T x^{(t)}, \\ \text{subject to} \quad & A^{(t)}x^{(t)} \geq b^{(t)}, \\ & x^{(t)} \in \{0,1\}^{l(t)}. \end{aligned}$$

This is a *rolling horizon approach*, and it can be also viewed as a *dynamic discrete tomography* problem.

One possible choice for $w^{(t)}$ is

$$\omega_{j_1}^{(t-1,t)} := \min_{j_2\,:\,\xi_{j_2}^{*\,(t-1)}=1} \{\mathrm{dist}(g_{j_1}^{(t)}, g_{j_2}^{(t-1)})\},$$

with $\mathrm{dist}(g_{j_1}^{(t)}, g_{j_2}^{(t-1)})$ denoting the distance (possibly but not necessarily Euclidean) between the two candidate grid points $g_{j_1}^{(t)}$ and $g_{j_2}^{(t-1)}$. Note that $\xi_{j_1}^{*\,(t-1)} = 1$ indicates that a particle is located at candidate grid point $g_{j_1}^{(t-1)}$. The algorithm thus prefers to fill candidate points that are (in some sense depending on dist) close to particles from the previous time step. If the initial distribution of particles is unknown, we can set $w^{(0)} := 0$ thereby giving no preference to any position.

The Euclidean distance function is a suitable choice for slowly moving particles. However, we can also incorporate momentum information (in fact, we do this in [H14]). If the particles, for instance, are known to move with a certain velocity, then a possible

choice would be

$$\mathrm{dist}(g_{j_1}^{(t)}, g_{j_2}^{(t-1)}) := \begin{cases} \sigma_1, & \text{for} \quad \rho_1 > ||g_{j_1}^{(t)} - g_{j_2}^{(t-1)}||_2, \\ \sigma_2, & \text{for} \quad \rho_1 \leq ||g_{j_1}^{(t)} - g_{j_2}^{(t-1)}||_2 \leq \rho_2, \\ \sigma_3, & \text{for} \quad \rho_2 < ||g_{j_1}^{(t)} - g_{j_2}^{(t-1)}||_2, \end{cases}$$

where ρ_1, ρ_2, σ_1, σ_2, σ_3 are prescribed non-negative numbers with $\sigma_2 < \min\{\sigma_1, \sigma_3\}$. A particle at $g_{j_1}^{(t-1)}$ thus most likely moves a distance between ρ_1 and ρ_2; no displacement direction is preferred in this example. (For a further discussion, see [H7].)

To test our approach we performed several numerical experiments. We also show that uniqueness of the solution can be detected in our algorithmic framework.

4.2 Applications

4.2.1 Plasma Physics: Results from [H14]

In [H14] we apply our rolling horizon approach from [H7] to real data (studying 3D slip velocities of a gliding arc discharge measured by a team of coauthors from plasma physics). Our particular application deals with the determination of the *slip velocity* of a *gliding arc discharge*. We will explain this briefly in the following lines.

An arc discharge is an electrical breakdown of a gas that produces an ongoing electrical discharge. The electrical current (in our case through air) produces a plasma, which is often referred to as *plasma column*. In a *gliding arc discharge* experiment, the string-like plasma column of the arc discharge is extended by a gas flow. In this way, non-thermal plasmas at atmospheric pressure can be generated. Applications can be found, for instance, in pollution control, combustion enhancement, sterilization, and surface treatment [28, 63, 72, 79]. For further details, see, e.g., [246]. The *slip velocity*, which is in our case the relative velocity between the plasma column and the gas flow, determines the convection cooling efficiency, the drag force, the electric field strength, and the radius of the conducting zone of the plasma column. Accurate measurements of the slip velocity and the length of the plasma column are essential to provide a better understanding of the gliding arc discharge. In previous studies, measurements of the slip velocity and the length of the plasma column were performed in 2D, i.e., by analyzing a single 2D camera image [187, 206] (for a discussion, see also [140]).

In our paper [H14], two high-speed cameras were synchronized to record images of the gliding arc in orthogonal imaging planes (two such images are shown in Fig. 6(a)). Employing our rolling horizon approach, we reconstructed the instantaneous 3D velocities of seven TiO_2 tracer particles illuminated by the plasma column. As the tracers are tiny (about 3 μm in diameter), they follow the motion of the gas flow and are therefore

suitable indicators for the local gas flow velocity. The plasma column and its velocity were also reconstructed in 3D (employing the so-called *snake model* from [42]). In particular, we determine here for the first time 3D slip velocities and 3D plasma column lengths for a gliding arc discharge. Reconstruction results are shown in Fig. 6(b).

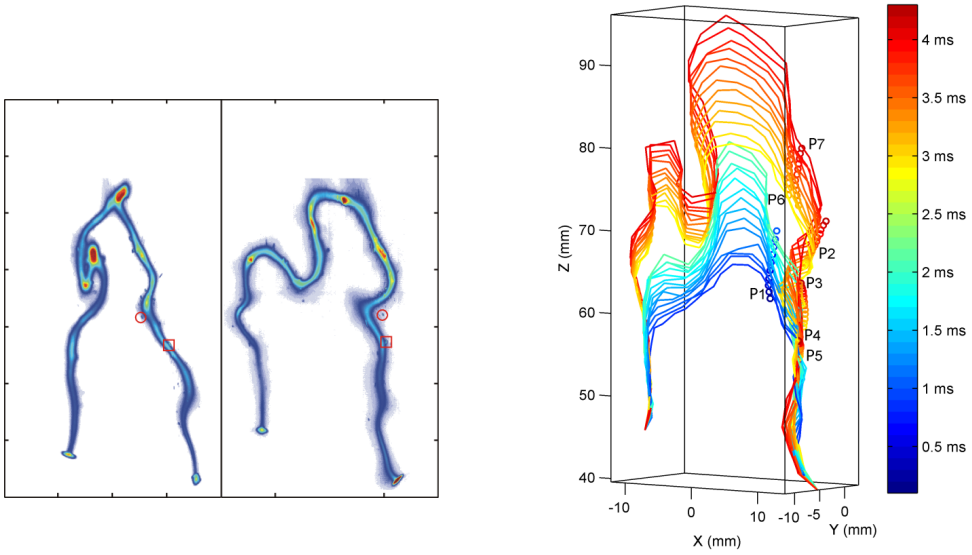

(a) **(b)**

Figure 6: Data and Reconstruction. (a) An image pair (real data) of the gliding arc discharge simultaneously recorded by the two high-speed cameras. In this image, two typical seeding particles illuminated by the bright plasma column are highlighted by a red square and circle located on the right hand-side part of the plasma column. (b) 3D plasma column and particle reconstruction. Trajectories of seven seeding particles are marked (P1 to P7). The colors indicate the time evolution from 0 to 4 ms.

Comparing with 2D results we conclude that previous studies might have underestimated the slip velocity by up to 80% and likewise the length of the plasma column by 25%. This, for instance, is cited by the authors of [104] to substantiate their findings that

> "the role of 'dragging' force from the electrode spots may be over-emphasized by some authors, e.g., [140], and the discharge elongation is caused mostly by nonuniform gas velocity distribution and presence of gas velocity components along the discharge channel. Thus, slip velocity can be also caused by other reasons [...]."

5 Tomographic Reconstructions of Polycrystals, [H1, H8, H10, H11, H13]

5.1 Theory, Algorithms, and Applications

The inverse problem of recovering polycrystal grain and orientation maps from X-ray diffraction data arises as an imaging problem in *materials science* (see, e.g, [7, 192]). Many materials, such as metals, ceramics and alloys, are composed of crystalline elements. These elements, called *grains*, might all share the same crystal lattice structure, but they typically differ in size, shape and orientation of the lattice. For *deformed* materials even the orientation might differ slightly within the grain. An image of the material at the grain level should therefore provide for each location x two quantities $f(x)$ and $o(x)$: the quantity $f(x)$ is the label of the grain that occupies x, while $o(x)$ is its orientation at x. Thus recovering an image at the grain level is equivalent to recovering the *grain map* f and the *orientation map* o, which both act as functions on the image domain.

5.1.1 Geometric Clustering, [H1]

In [H1] we consider the problem of reconstructing grain maps of undeformed materials from very few data that can be obtained from tomographic X-ray diffraction experiments (or which might be available as prior knowledge).

We introduce the concept of *generalized balanced power diagrams (GBPDs)*, where each grain is represented by (measured approximations of) its *center-of-mass (CMS)*, its *volume* and, if available, by its *second-order moments*. Such parameters may be obtained, for instance, from 3D X-ray diffraction experiments [192]. The exact global optimum of our model results from the solution of a suitable *linear program*. Our approach is, to our knowledge, the first method in this field that yields tessellations that are guaranteed to comply with measured grain volume information up to any required accuracy (within the present level of noise in the measurements). Based on verified real-world measurements, we show that from the few parameters per grain (3, respectively 6 in 2D and 4, respectively 10 in 3D) we obtain representations that coincide in $94-96\%$ of the pixels of the real grain map. We conclude that our approach seems to capture the physical principles governing the forming of such polycrystals in the underlying process quite well. Subsequent studies by Šedivý et al. [216, 217] and Spettl et al. [223] confirm our findings.

In the following we discuss our approach in some more detail.

For a positive definite matrix A we denote by $||\cdot||_A$ the *ellipsoidal norm*, defined by

$$||x||_A := \sqrt{x^T A x}. \tag{5}$$

Discussions of the use of ellipsoidal norms for modeling polycrystal structures can be found in [16, 29, 145].

Our aim is to reconstruct what we call *generalized balanced power diagrams (GBPDs)*. These diagrams generalize *power diagrams* (also known as *Laguerre* or *Dirichlet tessellations*), which in turn generalize *Voronoi diagrams*; see also [18] and [19, Sect. 6.2].

Any GBPD is specified by a set of distinct *sites* $S := \{s_1, \ldots, s_l\} \subseteq \mathbb{R}^d$, *additive weights* $(\sigma_1, \ldots, \sigma_l)^T \in \mathbb{R}^l$, and positive definite matrices $A_1, \ldots, A_l \in \mathbb{R}^{d\times d}$. The *j-th generalized balanced power cell* P_j is then defined by

$$P_j := \{x \in \mathbb{R}^d \,:\, ||x - s_j||^2_{A_j} - \sigma_j \leq ||x - s_k||^2_{A_k} - \sigma_k,\ \forall k \neq j\}.$$

The generalized balanced power diagram P is the l-tuple $P := (P_1, \ldots, P_l)$. We remark that power diagrams are obtained if the $A_1, \ldots, A_l$ are identity matrices, and if, in addition, $\sigma_1 = \cdots = \sigma_l = 0$, then we obtain Voronoi diagrams.

Somewhat surprising at first glance, GBPDs are closely related to optimal clusterings; see [39]. For this we introduce a particular clustering method that is based on solving a *weight-balanced least-squares assignment problem.*

This assignment problem is specified by a set of points $X := \{x_1, \ldots, x_m\} \subseteq \mathbb{R}^d$, sites $S := \{s_1, \ldots, s_l\} \subseteq \mathbb{R}^d$, weights $\omega_1, \ldots, \omega_m \in]0, \infty[$, positive definite matrices $A_1, \ldots, A_l \in \mathbb{R}^{d\times d}$, and cluster size bounds $\kappa^- := (\kappa_1^-, \ldots, \kappa_l^-)$, $\kappa^+ := (\kappa_1^+, \ldots, \kappa_l^+)$ with $0 < \kappa_j^- \leq \kappa_j^+$ and

$$\sum_{j=1}^{l} \kappa_j^- \leq \sum_{j=1}^{m} \omega_j \leq \sum_{j=1}^{k} \kappa_j^+.$$

The (fractional) *weight-balanced least-squares assignment problem* is the following linear optimization problem:

$$\begin{aligned}
&\text{(LP)} && \min \sum_{j=1}^{l}\sum_{k=1}^{m} \gamma_{j,k}\xi_{j,k} && \\
&\text{subject to} && \sum_{j=1}^{l} \xi_{j,k} = 1 && (k \in [m]),\\
& && \kappa_j^- \leq \sum_{k=1}^{m} \xi_{j,k}\omega_k \leq \kappa_j^+ && (j \in [l]),\\
& && \xi_{j,k} \geq 0 && (j \in [l];\ k \in [m]),
\end{aligned} \tag{6}$$

with $\gamma_{j,k} := \omega_k ||x_k - s_j||^2_{A_j}$ for all j, k. The $\xi_{j,k}$ are the variables; they specify the fraction of point x_k that is assigned to site s_j. Any optimal solution $C := (C_1, \ldots, C_l)$ of (6) where $C_j := (\xi_{j,1}, \ldots, \xi_{j,m})$ is called a *(fractional) weight-balanced least-squares assignment for X with sites $\{s_1, \ldots, s_l\}$*.

In the particular case of unit weights $(\omega_1, \ldots, \omega_m) = (1, \ldots, 1)$ we have a *totally unimodular* constraint matrix, which implies that 0/1-solutions can be found as basic feasible solutions in polynomial time (for definitions see, e.g., [213, Sect. 19.1] and [185, Def. 2.4]). We remark that voxelized maps can be obtained with this approach if the x_k represent voxels. In fact, $\xi_{j,k} = 1$ in a solution of (6) means that x_k belongs to the jth grain. These voxelized maps represent generalized balanced power diagrams (the additive weights $\sigma_1, \ldots, \sigma_l$ can be obtained as solutions of the dual linear program).

In the model introduced above, we optimize the objective function in (6), with fixed sites $s_1, \ldots, s_l$ (representing the measured CMS of the grains), and fixed values for the second-order moments, which (by (5)) define the metric for each grain. These second-order moments, or approximations thereof, can be obtained in favorable diffraction experiments (note that diffraction images record projections of the grains; by backprojecting the projections acquired from the same grain, an estimate of the corresponding second-order moments can be obtained). However, in our paper we utilize a *principal component analysis* [125] based on the original image in the following way: suppose for a set of points $\{g_1, \ldots, g_l\} \subseteq \mathbb{R}^d$ of a grain we are given the principal components $u_1, \ldots, u_d$ and corresponding eigenvalues $\lambda_1, \ldots, \lambda_d$ of the $d \times d$ covariance matrix of $G = (g_1, \ldots, g_l)$. The norm $|| \cdot ||_A$, where

$$A = U \Lambda^{-1} U^T \tag{7}$$

with $U = (u_1, \ldots, u_d)$ orthogonal and $\Lambda = \mathrm{diag}(\lambda_1, \ldots, \lambda_d)$ is an ellipsoidal norm for which $\{x \in \mathbb{R}^d : ||x||_A = 1\}$ defines an ellipsoid with semi-axes u_i of lengths $\sqrt{\lambda_i}$, $i = 1, \ldots, d$. The Euclidean norm is obtained in the special case where A equals the identity matrix. However, our algorithm can easily been extended using global techniques from [38] or local variants of [33].

It is worth noting that our approach generates by design (generalized balanced) power cells whose volumes (resp. areas) lie in the prescribed range. The centers of the cells, however, are not automatically guaranteed to coincide with $s_1, \ldots, s_l$.

We demonstrate in [H1] the favorable performance of our approach on several experimental data sets. A particular example is shown in Fig. 7, which depicts in black color the grain boundaries of a 2D aluminum sample imaged by *electron backscatter diffraction (EBSD)* [214]. The cell boundaries of the GBPDs obtained by our approach are shown in red and blue, respectively (for the blue solution second-order information was included). The original 339×339 pixel grain map contains 206 grains. Hence, for the blue solutions we employ $6 \cdot 206 = 1,236$ parameters (which is a reduction of

about two orders of magnitude compared to the total number of pixels of this image). The blue solution represents a rather close fit. In fact, 93.8% of the image pixels are resolved correctly (for comparison, the approach from [158] resolves here only 62.0% of the image pixels correctly).

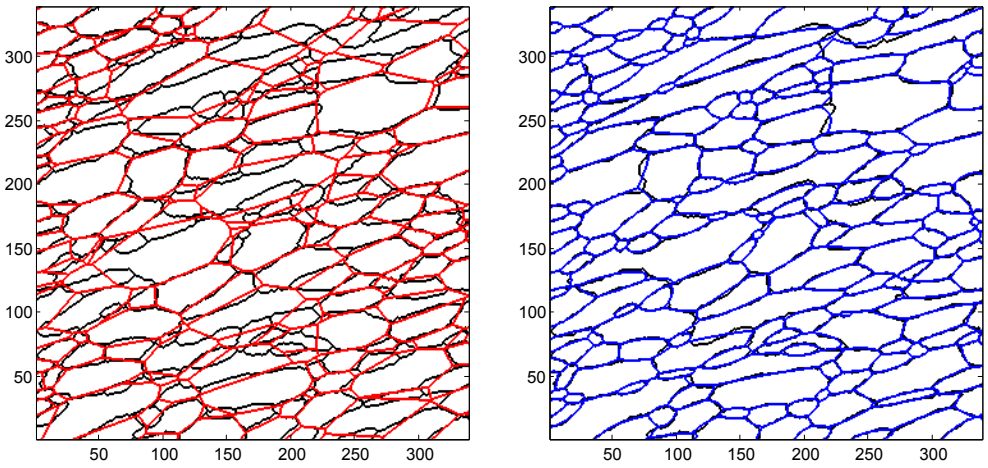

Figure 7: Tessellations of a real (EBSD) grain map, which contains many non-equiaxed grains. Real grain boundaries are shown in black, (a) the power diagram reconstruction is given in red, (b) the generalized balanced power diagram reconstruction is shown in blue.

We remark that GBPDs, as introduced in our paper, have also been found useful in the area of *stochastic geometry*. In the course of updating the 3rd edition of the book [48], Stoyan contacted us and proposed that we compare our algorithm to that from [231]. The following is a quote from [47].

> "Two teams, one formed by Andreas Alpers, Fabian Klemm and Peter Gritzmann, and the other by Kirubel Teferra, helped the authors of this book to carry out the following experiment: Using as data Figure 9.7 on page 353 [here Fig. 8; cells depicted in black color], which shows a Johnson-Mehl tessellation, the two teams reconstructed the tessellations with their programs independently. The better result was obtained by Alpers, Klemm and Gritzmann shown in Figure 9.A [here Fig. 8; cells depicted in blue color].
>
> The power of the algorithm of Alpers et al. (2015) is impressive: Though the tessellation in Figure 9.7 [here Fig. 8;] results from a process in which growth in the sites starts subsequently, the representation belongs to a model in which all sites start at the same instant!"

There is a large literature on crystal growth models such as the *Poisson–Voronoi*,

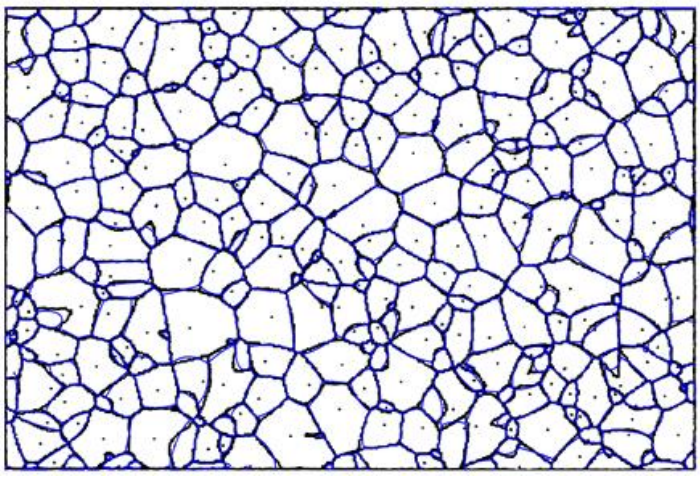

Figure 8: A tessellation obtained by a marked point process (black) and our reconstruction (blue). Taken from [47].

Johnson–Mehl and *Laguerre random tessellations* (see, e.g., [146, 234] and the literature cited therein). These models are typically considered as *random tessellation models*. For tessellations generated by *stationary marked Poisson processes*, see, e.g., [146, 147]. As our concept of GBPDs generalizes the concept of Laguerre tessellations, it seems interesting to study GBPDs also in the context of random tessellation models (see also the remark at the end of Sect. 5.1.2).

A rather different application is given in [40], where GBPDs are employed for the design of electoral districts where municipalities of a state have to be grouped into districts of nearly equal population while obeying certain politically motivated requirements.

5.1.2 Stochastic Algorithms, [H10, H11, H13]

In [H10] we focus on the task of reconstructing the grain map, assuming that the orientation map is known. In addition, we assume that $o(x) = o(y)$ holds for every x and y inside the same grain. Such grains are called *undeformed*. In [H11] we extend the approach to the case of *moderately* deformed grains, where we reconstruct f and o, allowing "small" differences between $o(x)$ and $o(y)$ if x and y are inside the same grain. In [H13] we develop an alternative method for the task of reconstructing moderately deformed grains. This alternative is an iterative method, similar to the *Algebraic Reconstruction Technique (ART)* [98] used in tomography (a fundamental difference is that here we reconstruct the function o, which does not map into the reals but into the group of *unit quaternions*, see, e.g., [17, Sect. 12]). The stochastic concept of

Gibbs priors [94] (see also [37, 239]) is incorporated in all our approaches serving as a *regularizing term* in the objective function. (Background information on stochastic regularizations of inverse problems can be found in the monographs [25, 103, 126, 229].)

We remark that prior to our work [H10], there existed no dedicated method for reconstructing grain or orientation maps from tomographic data. A major challenge is that, by diffraction, only very limited X-ray data (typically available for only 3-10 directions) can be acquired for each grain. Tomographic reconstructions using standard methods, as performed by Poulsen and Fu [193], yield noticeable gaps between neighboring grains of undeformed materials (see Fig. 9(b)). We show that such problems can be overcome by our dedicated methods. Moreover, our methods are the first that are capable of reconstructing grain and orientation maps of moderately deformed materials. Others have followed up on this line of research, see, for instance, [22, 24, 112, 150, 151, 194, 202, 225, 236]. More on the moderately deformed case can be found in [209] and the recent thesis [208] by Rodek.

Our methods developed in [H10, H11, H13] are stochastic, based on a modeling of grain maps (and orientation maps, respectively) as *Markov random fields* [37, 239]. A Markov random field is a finite set of random variables (the pixel variables in grain images of undeformed materials), where the conditional distribution of each variable depends only on the neighbor variables and the joint probability distribution (which, by the *Hammersley-Clifford theorem* [99, 109], will be a *Gibbs distribution*, to be defined further below) is completely characterized by the local conditional distributions. Originally motivated by questions from statistical physics (see the *Ising model* of ferromagentism [122] or its generalization, the *Potts model* [190]), Markov random field theory developed into a branch of probability theory that provides tools for analyzing spatial-temporal dependencies of physical phenomena (see, e.g., [92, 135, 239]). We apply this theory to model grain structures. The usefulness of Markov random fields for modeling grain structures has been reconfirmed in recent studies by Kumar et al. [144] and Acar and Sundararaghavan [1].

A stochastic model of images is characterized by a distribution function (also called *prior distribution*). For a Markov random field model this is a so-called *Gibbs distribution* (also known as *Boltzmann distribution*)

$$\pi(f) = \frac{1}{Z} e^{-H(f)/\beta}.$$

Here f is a (discretized) image, $H(f)$ is called the *energy function* and is represented as a weighted sum of *clique potentials* (for a precise definition, see [37, Sect. 7]; here it suffices to note that $H(f)$ has the form $H(f) = \sum_{j=1}^{k} V_j(f)$, for some natural number k and positive functions V_j depending on f only through the variables that lie in a specified neighborhood of a prescribed variable), β is a scaling factor, and Z is the *normalizing constant*, which ensures that π integrates to 1 over the support of π.

Estimating the parameters of a prior distribution is itself an inverse problem, which has been studied by many authors (see, e.g., [64, 105], [239, Sect. 17-19], and the literature cited therein). We estimate the parameters of the Gibbs distribution based on an estimator proposed by Derin and Elliot [59], which estimates the parameters from histogram data that has been acquired from typical sample collection of images (to avoid *inverse crimes* [53], the sample collection consists, in our case, of EBSD images of grains maps similar to the ones imaged in the experimental setup). Further discussions, in particular, for images that contain, as in grain images, piecewise homogeneous regions can be found in [149, 153]. For alternative estimators, see [2, 26, 32, 64].

We remark that the observed data in our application consists of a collection of diffraction images, which are recorded on a detector. The imaging model has been described in [192]. For the present purpose it suffices to note that we can assume that the observed data of the unknown grain map f is represented by a real-valued vector P_f whose components represent the recorded pixel intensities.

Allowing noise in the data, we define a *likelihood function* $\pi(P|f)$ that expresses our knowledge of how we expect our data P to look given that the true grain image is f. In our papers we consider

$$\pi_\alpha(P|f) = \frac{1}{Z'_\alpha} e^{-\alpha||P_f - P||_1},$$

with α and Z'_α denoting a real-valued parameter and the normalizing constant, respectively. We remark that our model allows also for other choices of likelihood functions. In our paper we experiment with different values of α (large values of α express high data fidelity).

Following the *Bayesian* paradigm, our aim is to estimate the *posterior distribution*

$$\pi_\alpha(f|P) = \frac{1}{Z''_\alpha} \pi_\alpha(P|f)\pi(f),$$

which represents the probability that f is the true grain image given that P has been observed (Z''_α denotes the normalizing constant). In our case, we are primarily interested in obtaining a *maximum posterior estimate*, i.e., we aim at recovering

$$f^* \in \arg\max_{f \in X} \pi_\alpha(f|P)$$

with X denoting the space of all (discretized) grain images. It should be noted, however, that, in principle, the Bayesian approach can also be used to recover other parameters of the distribution.

A problem with $\pi_\alpha(f|P)$ is that, due to the large image space, it is typically not possible to compute the normalizing constant Z''_α. Yet it is possible to sample from

$\pi_\alpha(f|P)$ by *Markov Chain Monte Carlo (MCMC)* methods. The basic idea behind MCMC methods is to construct a *Markov chain* whose *stationary distribution* is the desired sampling distribution $\pi_\alpha(f|P)$. The MCMC method that we employ is the *Metropolis algorithm*, which, developed by Metropolis and Ulam [170], Metropolis et al. [169], and Hastings [111], lies at the heart of at most MCMC methods. The Metropolis algorithm simulates the Markov chain, and if the Markov chain is simulated long enough by the Metropolis algorithm, then it will simulate draws from the posterior distribution. Theoretical convergence results can be found, in [222], [232], and [239, Sect. 10]. Estimating the finite-time behavior of a Markov chain, however, is generally a difficult task. Practical aspects are discussed in [55].

From the modeling point of view, the moderately deformed case differs only slightly form the undeformed case as now also the orientation map o needs to be recovered. This fits also into the previously described stochastic framework (now π is a function of f and o). The Gibbs prior that we use in the moderately deformed case is described in [H11, H13].

We remark that the use of Monte Carlo methods for the solution of inverse problems was already initiated in the 1960s by Keilis-Borok and Yanovskaya [132] and Press [195] (for a historical account, see [207]). Often, however, MCMC methods are found to be computationally too expensive to be of practical use for large data applications. That our algorithms are capable of handling real data results from the fact that we implemented several algorithmic ideas, sometimes borrowed from other fields, that speed up the computations. For instance, we represent the grain orientations by *quaternions* (more specifically, by *unit quaternions*, i.e., by elements $q \in \mathbb{H}$ that satisfy $||q||_2 = 1$). This allows us to take full advantage of the quaternion algebra, in which, for instance, compositions of orientations can be easily computed (via multiplication in $\mathbb{H}$). Another algorithmic idea, borrowed from discrete tomography [235], is that we represent (in certain steps of the Metropolis algorithm) the grain maps as binary images. The compact notation allows us to store several frequently used parameters (for instance, the so-called *transition probabilities* in the Metropolis algorithm) in several look-up tables, which can be kept in memory.

Figure 9 and 10 show to exemplary results obtained by our algorithms.

Figure 9 shows the error in the reconstruction for a 128×128-pixel phantom comprising 44 undeformed grains (the original phantom was obtained by the EBSD method). The left-hand side image shows the error (red and blue pixels) obtained by our stochastic approach in [H10]; the right-hand side image shows the error obtained by a previous method introduced by Poulsen and Fu [193].

Figure 10 shows the results of the two algorithms from [H11] and [H13] applied to a 64×64-pixel phantom, which comprises 26 moderately deformed grains. The algorithm

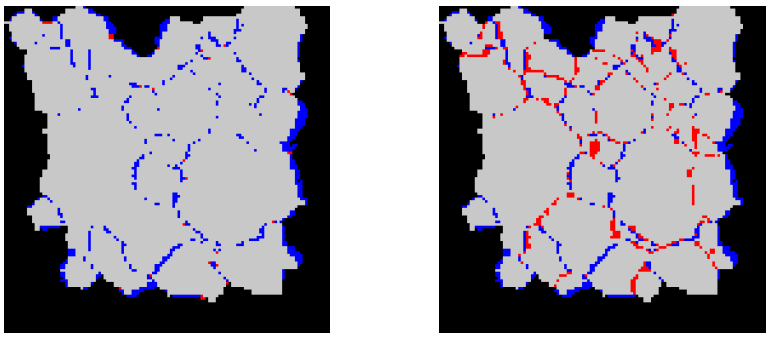

(a) **(b)**

Figure 9: (Adapted from [H10]) Error in the reconstruction of grain maps by two different methods: (a) Our Gibbs priors approach [H10]. (b) Approach from [193]. Erroneously assigned pixels in are indicated in red, wrong assignments in other parts — due to errors in the initial map — are indicated in blue. Gray pixels indicate correct assignments.

from [H13] recovers the test phantom exactly after a few seconds of computation time.

We remark that our Markov random field approach can be viewed as a stochastic approach for modeling grain maps using only a few parameters. The geometric clustering approach presented in Section 5.1.1 yields a different representations, which again involves only a few parameters. For future work it might seem interesting to work out the detailed connections.

5.1.3 Fourier Phase Retrieval, [H8]

Reconstructing a function from the modulus (i.e., absolute magnitudes) of its *Fourier transform (FT)* constitutes the well-known *Fourier phase retrieval problem*: the phase of the complex valued FT has to be retrieved before it can be inverted. This nonlinear inverse problem arises in optics, astronomy, crystallography (for *coherent X-rays*), and numerous other areas of physics and engineering [56, 124, 173], and is known as *binary phase retrieval problem* [154] if the function is 0/1-valued.

Motivated by the prospect that the newly developed technology of *X-ray free-electron lasers (XFELs)* [15, Section 2] will provide X-rays of unprecedented brilliance and coherence, we identify in [H8] a relevant mathematical model for tomographic (slice-by-slice based) grain imaging based on the physical principles of coherent X-ray diffraction. It turns out, that this problem can be viewed as the following generalization of the binary phase retrieval problem, which, to our knowledge it has not been considered

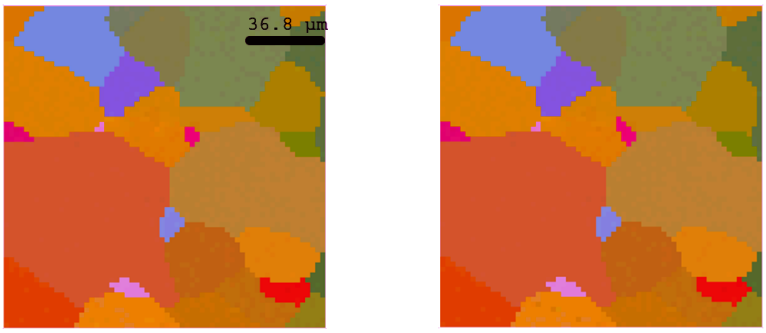

(a) **(b)**

Figure 10: Reconstruction of a moderately deformed orientation map from noiseless data (note that the data might not uniquely determine the solution). (a) Orientation map reconstructed by the approach from [H11]. (b) Orientation map reconstructed by the approach from [H13]. In this case, the approach from [H13] recovers the test phantom exactly. Different colors indicate different orientations.

in the literature before: the reconstruction of *multiple* 0/1-valued functions with non-overlapping bounded supports from moduli of *superpositions* of several displaced copies of their individual FTs. In other words, the two-dimensional version of the problem is the following (generalizations to higher dimensions are straightforward):

Problem 27 ([H8]).

For given $J, K \in \mathbb{N}$ and (displacement) vectors $t_{jk} \in \mathbb{R}^2$, $(j,k) \in [J] \times [K]$, the aim is to reconstruct the functions $f_j : \mathbb{R}^2 \to \{0,1\}$, $j \in [J]$, with non-overlapping bounded supports from the knowledge of

$$\left| \sum_{j=1}^{J} \sum_{k=1}^{K} \widehat{f_j}(\cdot - t_{jk}) \right|, \qquad (j,k) \in [J] \times [K]$$

where $\widehat{f_1}, \ldots, \widehat{f_J}$ denote the FTs of $f_1, \ldots, f_J$, respectively.

We call this variant the *binary superposed phase retrieval problem*. For $J = K = 1$, we obtain as special case the binary phase retrieval problem for a single object. However, we do not place any restrictions on the displacement vectors other than that they should be known, and thus the problem usually does not reduce to the binary phase retrieval problem. Figure 11 shows the modulus of $K = 14$ superposed FTs of $J = 2$ binary functions (representing two grains; for detailed information, see [H8]). Note that in grain imaging, each of the $f_1, \ldots, f_J$ represents the grain map of a single (undeformed) grain.

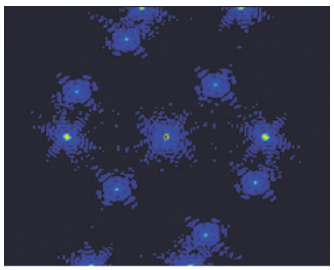

Figure 11: Modulus of 14 superposed FTs of two binary functions (the origin of the axes is located in the center of the image; lighter colors represent larger absolute values).

Binary superposed phase retrieval poses major algorithmic challenges. Standard phase retrieval algorithms (see, e.g., [120]) aim at reconstructing a single function from its FT modulus. Thus only a *superposed* function would be returned as output from such an algorithm that is applied to superposed FT modulus data. We aim, however, at reconstructing the individual binary functions – and this is the major algorithmic challenge.

In [H8] we develop the first two algorithms for Probl. 27. Our first algorithm, *Algorithm I*, follows the general paradigm of *Metropolis-based Monte Carlo methods* [169]. *Algorithm II*, on the other hand, represents an adaptation of the *Hybrid-Input-Output (HIO)* algorithm [75], which is frequently used for standard phase retrieval problems. While Algorithm I aims at reconstructing the individual functions simultaneously, Algorithm II proceeds sequentially.

We are not going into the details of Algorithm I here as they are given in [H8]. We remark, however, that Algorithm I can be seen as an adaptation of the Gibbs-prior approach that we developed in [H10, H11, H13, 14] for the task of reconstructing grain maps from tomographic diffraction data acquired by *incoherent X-rays*. The main difference from the algorithms presented in those papers is that here we use a different forward operator (the non-linear operator maps the binary functions to the modulus of their superposed FTs). Our Algorithm I is more time efficient than other comparable Monte Carlo methods, because we make use of the fact that the functions to be reconstructed are binary (in fact, this allows us to introduce a fast updating step for the computation of the Fourier transform, which is performed in each iteration of the algorithm).

The idea behind our Algorithm II is briefly described as follows. Standard phase retrieval methods reconstruct single functions from single FTs. In certain cases we can reconstruct the $f_1, \ldots, f_J$ independently. For example, if for each $j' \in [J]$ there is an

index $k' \in [K]$ such that, for all u in a neighborhood of $t_{j'k'}$, we have

$$\left| \sum_{j=1}^{J} \sum_{k=1}^{K} \widehat{f}_j(u - t_{jk}) \right| \approx \left| \widehat{f}_{j'}(u - t_{j'k'}) \right| \tag{8}$$

then, in principle, $f_{j'}$ can be recovered from the data using a phase retrieval method. This single reconstruction (cycling through all $j \in [J]$) is performed by our Algorithm II (of course, (8) is a valid approximation only in special scattering situations in which superposition effects from different FTs are small). As a subroutine the already mentioned HIO algorithm is used, which is basically an iterative method following the *Gerchberg-Saxton scheme* [93] for reconstructing a single function from its FT modulus.

The two algorithms introduced in our paper are, to our knowledge, the first algorithms for binary superposed phase retrieval.

6 Geometric Methods for Electron Tomography, [H2]

6.1 Algorithms and Applications in Materials Science

The term *electron tomography (ET)* refers generally to any tomographic technique that employs the *transmission electron microscope (TEM)* for data collection (typically, by tilting the object in multiple directions); see [78, 139]. Mathematically speaking, the main task is here again to invert the *Radon or X-ray transform* (see also [201]). However, particularly in materials science application [171] the image quality obtained by standard inversion methods (such as *filtered backprojection*; see, e.g., [177, Sect. 5.1] and [127, Sect. 3.6]) is seriously affected by the problems of *missing wedge artefacts* and *non-linear projection intensities due to diffraction effects*. The former refers to the fact that data cannot be acquired over the full 180° tilt range; the latter implies that for some orientations, crystalline structures can show strong contrast changes. Nevertheless, standard methods are still widely used due to an apparent lack of alternatives [73, 183].

However, alternatives exist in the mathematical literature. *Geometric tomography* [83], for instance, is concerned in part with the tomographic reconstruction of homogeneous (i.e., geometric) objects. Similarly, *discrete tomography* [115, 116] usually deals with objects for which atomicity is a constraint or objects that exhibit a small number of attenuation coefficients. In many applications, certain prior knowledge about the shape of the structure of interest is available. For example, when reconstructing nanorods, nanowires or certain types of nanoparticles, one can typically assume that the structures are convex. In particular, in our experimental application of reconstructing an InAs nanowire from *high-angle annular dark-field scanning transmission electron microscopy (HAADF STEM)* data [H2, 188], it is known that the object is comprised

of cross-sections that are mostly close to regular hexagons; see [61, 237] (for differently shaped polygonal cross-sections, see, e.g., [131, 157, 205]).

6.1.1 Results from [H2]

In [H2] we demonstrate the use of geometric prior knowledge to overcome the problems of missing wedge and non-linear intensities due to diffraction effects by introducing four algorithms. One of the algorithms ($2n$-GON) appears in [H2] for the first time and uses the strongest geometric prior knowledge available in our setup, namely that the slices contain nearly regular hexagons. Two algorithms, GKXR and MPW, are introduced for the first time in the ET context and another algorithm (DART) is applied for the first time to the reconstruction of a nanowire. As a fifth method, we discuss in [H2] the BART algorithm [114], which was introduced in the 1970s and performs very well on homogeneous objects. BART has been implemented in the open-source software SNARK09 [138], and in [H2] we provide commands and parameters that yield high quality reconstructions in our context.

Without going into details, we would like to comment briefly on two of our methods, which can be called *object-based* since the routines aim at determining a small number of parameters that completely describe the object (in our case, the vertices of polytopes). The Handbook of Mathematical Methods in Imaging [181, p. 1013] refers to the two methods as *"other reconstruction schemes."*

The *Gardner-Kiderlen X-ray (GKXR)* algorithm [88] is an algorithm from the field of geometric tomography. It arose from theoretical work [90] in which it was shown that there are certain sets of four directions in 2D such that the exact X-rays of a 2D convex object in these directions determine it uniquely among all 2D convex shapes. Our work [H2] represents the first implementation of this algorithm (a main step of the algorithm involves solving a heavily non-linear optimization problem). More details can be found in [88].

The *modified Prince-Willsky (MPW)* algorithm [87], reconstructs a convex object K from its *support function* h_K, which takes a direction (unit vector u) as input and returns a number that corresponds to the extent of K in direction u. (More precisely, $h_K(u) := \max_{x \in K} u^T x$, with $u^T x$ denoting the inner product of u and x.) The convex object K is completely determined by its support function values in all directions (see [83, Sect. 0.6]). Under mild restrictions (the sequence of employed directions u needs to be "evenly spread"), the output of the algorithm converges almost surely as the number of projections, affected by Gaussian noise of fixed variance, approaches infinity [89]. Our implementation of MPW employs the Xpress® solver [74] for solving quadratic programs.

Along with simulations, we perform in [H2] reconstructions from real-world data. The data (see Fig. 12) is obtained via *high-angle annular dark-field scanning transmission electron microscopy (HAADF STEM)* from the nanowire shown in Fig. 1(b).

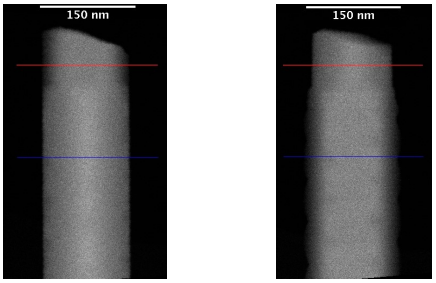

(a) **(b)**

Figure 12: Nanowire data: (a,b) 2-dimensional HAADF STEM images taken from the tilt series of the 3-dimensional wire at two different angles.

Reconstructions of the nanowire using the different algorithms are shown in Fig. 13.

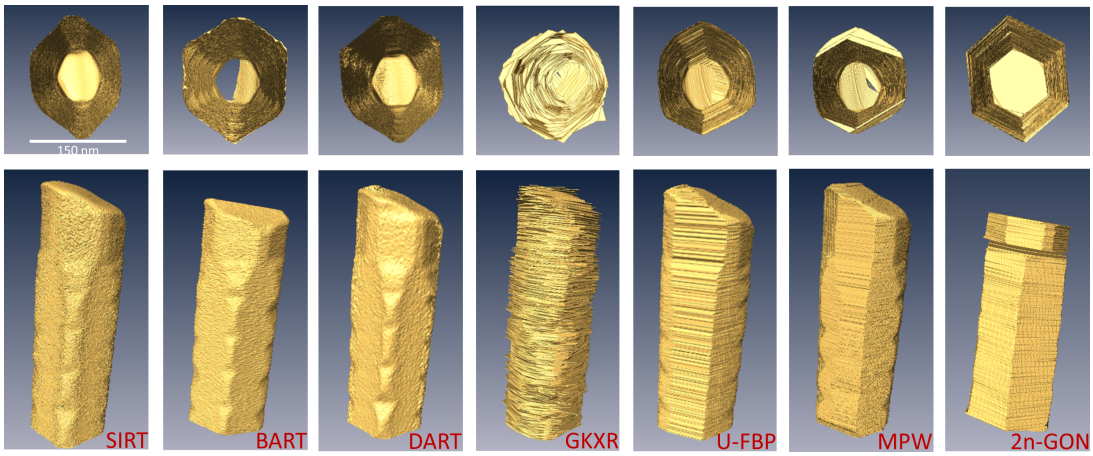

Figure 13: Reconstruction of the nanowire using different algorithms. Top-to-bottom and frontal views are shown in the first and second row, respectively. GKXR requires only X-ray data from 4 directions; U-FBP, MPW, and 2n-GON reconstruct from projections.

Papers Included in This Thesis

[H1] A. Alpers, A. Brieden, P. Gritzmann, A. Lyckegaard, and H. F. Poulsen. "Generalized balanced power diagrams for 3D representations of polycrystals". In: *Phil. Mag.* 95.9 (2015), pp. 1016–1028.

[H2] A. Alpers, R. J. Gardner, S. König, R. S. Pennington, C. B. Boothroyd, L. Houben, R. E. Dunin-Borkowski, and K. J. Batenburg. "Geometric reconstruction methods for electron tomography". In: *Ultramicroscopy* 128.C (2013), pp. 42–54.

[H3] A. Alpers and P. Gritzmann. "Dynamic discrete tomography". submitted to Inverse Probl. 2017.

[H4] A. Alpers and P. Gritzmann. "On double-resolution imaging and discrete tomography". under revision, *SIAM J. Discrete Math.*, http://arxiv.org/abs/1701.04399. 2017.

[H5] A. Alpers and P. Gritzmann. "On stability, error correction, and noise compensation in discrete tomography". In: *SIAM J. Discrete Math.* 20.1 (2006), pp. 227–239.

[H6] A. Alpers and P. Gritzmann. "Reconstructing binary matrices under window constraints from their row and column sums". In: *Fund. Inf.* 155.4 (2017), pp. 321–340.

[H7] A. Alpers, P. Gritzmann, D. Moseev, and M. Salewski. "3D particle tracking velocimetry using dynamic discrete tomography". In: *Comput. Phys. Commun.* 187.1 (2015), pp. 130–136.

[H8] A. Alpers, G. T. Herman, H. F. Poulsen, and S. Schmidt. "Phase retrieval for superposed signals from multiple binary objects". In: *J. Opt. Soc. Am. A* 27.9 (2010), pp. 1927–1937.

[H9] A. Alpers and D. G. Larman. "The smallest sets of points not determined by their x-rays". In: *Bull. Lond. Math. Soc.* 47.1 (2015), pp. 171–176.

[H10] A. Alpers, H. F. Poulsen, E. Knudsen, and G. T. Herman. "A discrete tomography algorithm for improving the quality of 3DXRD grain maps". In: *J. Appl. Crystallogr.* 39.4 (2006), pp. 582–588.

[H11] A. Alpers, L. Rodek, H. F. Poulsen, E. Knudsen, and G. T. Herman. "Discrete tomography for generating grain maps of polycrystals". In: *Advances in discrete tomography and its applications*. Ed. by G. T. Herman and A. Kuba. Birkhäuser, Boston, 2007, pp. 271–301.

[H12] A. Alpers and R. Tijdeman. "The two-dimensional Prouhet-Tarry-Escott problem". In: *J. Number Theory* 123.2 (2007), pp. 403–412.

[H13] A. K. Kulshreshth, A. Alpers, G. T. Herman, E. Knudsen, L. Rodek, and H. F. Poulsen. “A greedy method for reconstructing polycrystals from three-dimensional x-ray diffraction data”. In: *Inverse Probl. Imaging* 3.1 (2009), pp. 69–85.

[H14] J. Zhu, J. Gao, A. Ehn, M. Aldén, Z. Li, D. Moseev, Y. Kusano, M. Salewski, A. Alpers, P. Gritzmann, and M. Schwenk. “Measurements of 3D slip velocities and plasma column lengths of a gliding arc discharge”. In: *Appl. Phys. Lett.* 106.4 (2015), pp. 044101-1–4.

Other References

[1] P. Acar and V. Sundararaghavan. "A Markov random field approach for modeling spatio-temporal evolution of microstructures". In: *Modelling Simul. Mater. Sci. Eng.* 24.7 (2016), p. 075005.

[2] C. O. Acuna. "Texture modeling using Gibbs distributions". In: *CVGIP-Graph. Model Im.* 54.3 (1992), pp. 210–222.

[3] A. Adler and S.-Y. R. Li. "Magic cubes and Prouhet sequences". In: *Amer. Math. Monthly* 84.8 (1977), pp. 618–627.

[4] R. Adrian. "Multi-point optical measurements of simultaneous vectors in unsteady flow—a review". In: *Int. J. Heat Fluid Flow* 7.2 (1986), pp. 127–145.

[5] R. J. Adrian and J. Westerweel. *Particle Image Velocimetry*. Cambridge University Press, New York, 2011. ISBN: 978-0-521-44008-0.

[6] J. Aliste-Prieto, A. de Mier, and J. Zamora. "On trees with the same restricted U-polynomial and the Prouhet-Tarry-Escott problem". In: *Discrete Math.* 340.6 (2017), pp. 1435–1441.

[7] A. Alpers. "A short introduction to tomographic grain map reconstruction". In: *PU.M.A.* 20.1-2 (2009), pp. 157–163.

[8] A. Alpers. "Instability and Stability in Discrete Tomography". (published by Shaker Verlag, ISBN 3-8322-2355-X). PhD thesis. Zentrum Mathematik: Technische Universität München, 2003.

[9] A. Alpers and S. Brunetti. "On the stability of reconstructing lattice sets from X-rays along two directions". In: *Discrete geometry for computer imagery*. Vol. 3429. Lecture Notes in Computer Science. Springer, Berlin, 2005, pp. 92–103.

[10] A. Alpers and S. Brunetti. "Stability results for the reconstruction of binary pictures from two projections". In: *Image Vision Comput.* 25.10 (2007), pp. 1599–1608.

[11] A. Alpers and P. Gritzmann. "On the degree of ill-posedness in discrete tomography". manuscript. 2017.

[12] A. Alpers, P. Gritzmann, and S. Fraß (support). *Calendar Image, 1 of 12 winners of the image competition for the German Research Foundation (DFG) Calendar 2014*. Mathematical artwork, DFG. Available at http://www.dfg.de/dfg_magazin/aus_der_wissenschaft/archiv/mathe_kalender2014/1411_november/index.html. 2014.

[13] A. Alpers, P. Gritzmann, and L. Thorens. “Stability and instability in discrete tomography”. In: *Digital and image geometry*. Vol. 2243. Lecture Notes in Computer Science. Berlin: Springer, 2001, pp. 175–186.

[14] A. Alpers, E. Knudsen, H. F. Poulsen, and G. T. Herman. “Resolving ambiguities in reconstructed grain maps using discrete tomography”. In: *Electron. Notes Discrete Math.* 20.1 (2005), pp. 419–437.

[15] J. Als-Nielsen and D. McMorrow. *Elements of Modern X-Ray Physics*. Wiley, Chichester, 2001. ISBN: 0-471-498572.

[16] H. Altendorf, F. Latourte, D. Jeulin, M. Faessel, and L. Saintoyant. “3D reconstruction of a multiscale microstructure by anisotropic tessellation models”. In: *Image Anal. Stereol.* 33.2 (2014), pp. 121–130.

[17] S. L. Altmann. *Rotations, Quaternions, and Double Groups*. Clarendon Press, Oxford, 1986. ISBN: 0-486-44518-6.

[18] F. Aurenhammer. “Power diagrams: properties, algorithms and applications”. In: *SIAM J. Comput.* 16.1 (1987), pp. 78–96.

[19] F. Aurenhammer, R. Klein, and D.-T. Lee. *Voronoi Diagrams and Delaunay Triangulations*. World Scientific, Singapore, 2013. ISBN: 978-981-4447-63-8.

[20] J. Banhart. *Advanced Tomographic Methods in Materials Research and Engineering*. Oxford University Press, Oxford, 2008. ISBN: 978-0199213245.

[21] R. Barabash and G. Ice, eds. *Strain and Dislocation Gradients from Diffraction: Spatially-Resolved Local Structure and Defects*. World Scientific, Singapore, 2014. ISBN: 978-1-908979-62-9.

[22] N. R. Barton and J. V. Bernier. “A method for intragranular orientation and lattice strain distribution determination”. In: *J. Appl. Crystallogr.* 45.6 (2012), pp. 1145–1155.

[23] L. Bastien. “Impossibilité de $u + v \overset{3}{=} x + y + z$”. In: *Sphinx-Oedipe* 8.1 (1913), pp. 171–172.

[24] K. J. Batenburg, J. Sijbers, H. F. Poulsen, and E. Knudsen. “DART: a robust algorithm for fast reconstruction of three-dimensional grain maps”. In: *J. Appl. Crystallogr.* 43.6 (2010), pp. 1464–1473.

[25] M. Bertero and P. Boccacci. *Introduction to Inverse Problems in Imaging*. IOP Publishing, Bristol, 1998. ISBN: 0-7503-0439-1.

[26] J. Besag. “Spatial interaction and the statistical analysis of lattice systems”. In: *J. R. Stat. Soc. Series B Stat. Methodol.* 36.2 (1974), pp. 192–236.

[27] O. Bill, M. Faouzi, R. Meuli, P. Maeder, M. Wintermark, and P. Michel. “Added value of multimodal computed tomography imaging: analysis of 1994 acute ischaemic strokes”. In: *Eur. J. Neurol.* 24.1 (2017), pp. 167–174.

[28] Z. Bo, E. Wu, J. Yan, Y. Chi, and K. Cen. "Note: Gliding arc discharges with phase-chopped voltage supply for enhancement of energy efficiency in volatile organic compound decomposition". In: *Rev. Sci. Instrum.* 84.1 (2013), p. 016105.

[29] J.-D. Boissonnat, C. Wormser, and M. Yvinec. "Anisotropic diagrams: the Labelle Shewchuk approach revisited". In: *Theor. Comput. Sci.* 408.2-3 (2008), pp. 163–173.

[30] E. D. Bolker, C. Offner, R. Richman, and C. Zara. "The Prouhet-Tarry-Escott problem and generalized Thue-Morse sequences". In: *J. Comb.* 7.1 (2016), pp. 117–133.

[31] B. Borchert, P. McKenzie, and K. Reinhardt. "Few product gates but many zeroes". In: *Chicago J. Theoret. Comput. Sci.* 2013.2 (2013), pp. 1–22.

[32] C. F. Borges. "On the estimation of Markov Random Field Parameters". In: *IEEE Trans. Pattern Anal. Mach. Intell.* 21.3 (1999), pp. 216–224.

[33] S. Borgwardt, A. Brieden, and P. Gritzmann. "An LP-based k-means algorithm for balancing weighted point sets". In: *Eur. J. Oper. Res.* 263.2 (2017), pp. 349–355.

[34] P. Borwein. *Computational Excursions in Analysis and Number Theory*. Springer, New York, 2002. ISBN: 0-387-95444-9.

[35] P. Borwein and C. Ingalls. "The Prouhet-Tarry-Escott problem revisited". In: *Enseign. Math.* 40.1-2 (1994), pp. 3–27.

[36] P. Borwein, P. Lisoněk, and C. Percival. "Computational investigations of the Prouhet-Tarry-Escott Problem". In: *Math. Comp.* 72.244 (2003), pp. 2063–2070.

[37] P. Brémaud. *Markov Chains: Gibbs Fields, Monte Carlo Simulation, and Queues*. Springer, New York, 1999. ISBN: 0-387-98509-3.

[38] A. Brieden and P. Gritzmann. "On clustering bodies: geometry and polyhedral approximation". In: *Discrete Comput. Geom.* 44.1 (2010), pp. 508–534.

[39] A. Brieden and P. Gritzmann. "On optimal weighted balanced clusterings: gravity bodies and power diagrams". In: *SIAM J. Discrete Math.* 26.2 (2012), pp. 415–434.

[40] A. Brieden, P. Gritzmann, and F. Klemm. "Constrained clustering via diagrams: A unified theory and its applications to electoral district design". In: *Eur. J. Oper. Res.* 263.1 (2017), pp. 18–34.

[41] S. Brunetti, P. Dulio, L. Hajdu, and C. Peri. "Ghosts in discrete tomography". In: *J. Math. Imaging Vision* 53.2 (2015), pp. 210–224.

[42] Y. Cai, Z. Su, Z. Li, R. Sun, X. Liu, and Y. Zhao. “Two-view curve reconstruction based on the snake model”. In: *J. Comput. Appl. Math.* 236.5 (2011), pp. 631–639.

[43] T. Caley. “The Prouhet-Tarry-Escott problem”. PhD thesis. Department of Pure Mathematics: University of Waterloo, 2012.

[44] T. Caley. “The Prouhet-Tarry-Escott problem for Gaussian integers”. In: *Math. Comp.* 82.282 (2013), pp. 1121–1137.

[45] A. Černý. “On Prouhet’s solution to the equal powers problem”. In: *Theor. Comput. Sci.* 491.17 (2013), pp. 33–46.

[46] S.-K. Chang. “The reconstruction of binary patterns from their projections”. In: *Comm. ACM* 14.1 (1971), pp. 21–25.

[47] S. N. Chiu, D. Stoyan, W. Kendall, and J. Mecke. *Accompanying web page for the book: Stochastic Geometry and its Applications, 3rd edition*. http://www.math.hkbu.edu.hk/~snchiu/cskm/cskm2013.html. [Accessed: 2017-11-03].

[48] S. N. Chiu, D. Stoyan, W. Kendall, and J. Mecke. *Stochastic Geometry and its Applications*. 3rd edition. Wiley, Chichester, 2013. ISBN: 978-0470664810.

[49] A. Choudhry. “A new approach to the Tarry-Escott problem”. In: *Int. J. Number Theory* 13.2 (2017), pp. 393–417.

[50] A. Choudhry. “Matrix analogues of the Tarry-Escott problem, multigrade chains and the equation of Fermat”. In: *Math. Student* 75.1-4 (2006), pp. 215–224.

[51] A. Choudhry and J. Wróblewski. “Ideal solutions of the Tarry-Escott problem of degree eleven with applications to sums of thirteenth powers”. In: *Hardy-Ramanujan J.* 31.1 (2008), pp. 1–13.

[52] M. Cipu. “Upper bounds for norms of products of binomials”. In: *LMS J. Comput. Math.* 7.1 (2004), pp. 37–49.

[53] D. Colton and R. Kress. *Inverse acoustic and electromagnetic scattering theory*. Springer, Berlin, 1992. ISBN: 978-1-4614-4941-6.

[54] S. A. Cook. “The complexity of theorem-proving procedures”. In: *Proc. 3rd Ann. ACM Symp. Theory of Computing*. ACM. 1971, pp. 151–158.

[55] M. K. Cowles and B. P. Carlin. “Markov Chain Monte Carlo Convergence Diagnostics: A Comparative Review”. In: *J. Am. Stat. Assoc.* 91.434 (1996), pp. 883–904.

[56] J. C. Dainty and J. R. Fienup. “Phase Retrieval and Image Reconstruction for Astronomy”. In: *Image Recovery: Theory and Application*. Ed. by H. Stark. Academic Press, Orlando, 1987, pp. 231–275.

[57] B. van Dalen. “Stability results for uniquely determined sets from two directions in discrete tomography”. In: *Discrete Math.* 309.12 (2009), pp. 3905–3916.

[58] R. Dalitz, S. Petra, and C. Schnörr. “Compressed Motion Sensing”. In: *Proc. SSVM*. Vol. 10302. LNCS. Springer, 2017, pp. 602–613.

[59] H. Derin and H. Elliott. “Modeling and segmentation of noisy and textured images using Gibbs random fields”. In: *IEEE Trans. Pattern Anal. Mach. Intell.* 9.1 (1987), pp. 39–55.

[60] Z. Di, S. Leyffer, and S. M. Wild. “Optimization-Based Approach for Joint X-Ray Fluorescence and Transmission Tomographic Inversion”. In: *SIAM J. Imaging Sciences* 9.1 (2016), pp. 1–23.

[61] K. A. Dick. “A review of nanowire growth promoted by alloys and non-alloying elements with emphasis on Au-assisted III-V nanowires”. In: *Prog. Cryst. Growth. Charact. Mater.* 54.1–3 (2008), pp. 138–173.

[62] L. E. Dickson. *History of the Theory of Numbers*. Vol. 2. Dover Publications, Mineola, 1920. ISBN: 0-486-44233-0.

[63] C. M. Du, J. Wang, L. Zhang, H. X. Li, H. Liu, and Y. Xiong. “The application of a non-thermal plasma generated by gas-liquid gliding arc discharge in sterilization”. In: *New J. Phys.* 14.1 (2012), p. 013010.

[64] R. C. Dubes and A. K. Jain. “Random field models in image analysis”. In: *J. Appl. Stat.* 16.2 (1989), pp. 131–164.

[65] P. Dulio, R. J. Gardner, and C. Peri. “Discrete point X-rays”. In: *SIAM J. Discrete Math.* 20.1 (2006), pp. 171–188.

[66] C. Dürr, F. Guiñez, and M. Matamala. “Reconstructing 3-Colored Grids from Horizontal and Vertical Projections is NP-Hard: A Solution to the 2-Atom Problem in Discrete Tomography”. In: *SIAM J. Discrete Math* 26.1 (2012), pp. 330–352.

[67] P. Erdős and G. Szekeres. “On the product $\prod_{k=1}^{n}(1 - z^{a_k})$”. In: *Acad. Serbe Sci. Publ. Inst. Math.* 13.1 (1959), pp. 29–34.

[68] E. B. Escott. “The calculation of logarithms”. In: *Quart. J. Math.* 41.2 (1910), pp. 147–167.

[69] L. Euler. “Letter to Goldbach, Sept 4, 1751”. In: *Corresp. Math. Phys. (ed. Fuss)*. Vol. 1. http://eulerarchive.maa.org/correspondence/. St. Petersburg, 1843, pp. 549–552.

[70] European XFEL. *Official Webpage*. http://www.xfel.eu/de/. [Accessed: 2017-11-03].

[71] European XFEL. *Scientific Instrument MID*. https://www.xfel.eu/facility/instruments/mid/index_eng.html. [Accessed: 2017-11-03].

[72] Z. Feng, N. Saeki, T. Kuroki, M. Tahara, and M. Okubo. “Surface modification by nonthermal plasma induced by using magnetic-field-assisted gliding arc discharge”. In: *Appl. Phys. Lett.* 101.4 (2012), pp. 041602-1–4.

[73] J.-J. Fernandez. “Computational methods for electron tomography”. In: *Micron* 43.10 (2012), pp. 1010–1030.

[74] FICO™. *Xpress Optimization Suite*. http://www.fico.com. [Accessed: 2017-11-03].

[75] J. R. Fienup. “Phase Retrieval Algorithms: A Comparison”. In: *J. Opt. Soc. Am. A* 21.15 (1982), pp. 2758–2769.

[76] M. Filaseta and M. Markovich. “Newton polygons and the Prouhet-Tarry-Escott problem”. In: *J. Number Theory* 174.1 (2017), pp. 384–400.

[77] P. C. Fishburn, J. C. Lagarias, J. A. Reeds, and L. A. Shepp. “Sets uniquely determined by projections on axes II: Discrete case”. In: *Discrete Math.* 91.2 (1991), pp. 149–159.

[78] J. Frank. *Electron Tomography: Methods for Three-Dimensional Visualization of Structures in the Cell*. Springer, New York, 2006. ISBN: 978-0-387-31234-7.

[79] A. Fridman, A. Gutsol, S. Gangoli, Y. Ju, and T. Ombrello. “Characteristics of Gliding Arc and Its Application in Combustion Enhancement”. In: *J. Propul. Power* 24.6 (2008), pp. 1216–1228.

[80] M. Frolov. “Égalités à deux degrés”. In: *Bull. Soc. Math. France* 17.1 (1889), pp. 69–83.

[81] D. Gale. “A theorem on flows in networks”. In: *Pacific J. Math.* 7.2 (1957), pp. 1073–1082.

[82] V. Gandikota, B. Ghazi, and E. Grigorescu. “NP-Hardness of Reed-Solomon Decoding, and the Prouhet-Tarry-Escott Problem”. In: *IEEE 57th Annual Symposium on Foundations of Computer Science (FOCS)*. Vol. 1. IEEE, 2016, pp. 760–769.

[83] R. J. Gardner. *Geometric Tomography*. 2nd edition. Cambridge University Press, New York, 2006. ISBN: 978-0-521-68493-4.

[84] R. J. Gardner and P. Gritzmann. “Discrete tomography: Determination of finite sets by X-rays”. In: *Trans. Amer. Math. Soc.* 349.6 (1997), pp. 2271–2295.

[85] R. J. Gardner, P. Gritzmann, and D. Prangenberg. “On the computational complexity of determining polyatomic structures by X-rays”. In: *Theoret. Comput. Sci.* 233.1-2 (2000), pp. 91–106.

[86] R. J. Gardner, P. Gritzmann, and D. Prangenberg. “On the computational complexity of reconstructing lattice sets from their X-rays”. In: *Discrete Math.* 202.1-3 (1999), pp. 45–71.

[87] R. J. Gardner and M. Kiderlen. “A new algorithm for 3D reconstruction from support functions”. In: *IEEE Trans. Pattern Anal. Mach. Intell.* 31.3 (2009), pp. 556–562.

[88] R. J. Gardner and M. Kiderlen. “A solution to Hammer’s X-ray reconstruction problem”. In: *Adv. Math.* 214.1 (2007), pp. 323–343.

[89] R. J. Gardner, M. Kiderlen, and P. Milanfar. “Convergence of algorithms for reconstructing convex bodies and directional measures”. In: *Ann. Statist.* 34.3 (2006), pp. 1331–1374.

[90] R. J. Gardner and P. McMullen. “On Hammer’s X-ray problem”. In: *J. London Math. Soc. (2)* 21.1 (1980), pp. 171–175.

[91] M. R. Garey and D. S. Johnson. *Computers and Intractability*. W. H. Freeman and Co., San Francisco, 1979. ISBN: 0-7167-1045-5.

[92] H.-O. Georgii. *Gibbs Measures and Phase Transitions*. De Gruyter Studies in Mathematics. de Gruyter, Berlin, 1988. ISBN: 0-89925-462-4.

[93] R. W. Gerchberg and W. O. Saxton. “A practical algorithm for the determination of phase from image and diffraction plane pictures”. In: *Optik* 35.2 (1972), pp. 237–246.

[94] W. Gibbs. *Elementary Principles of Statistical Mechanics*. Reprint of the 1902 original. Dover Publications Inc., Mineola, 2014. ISBN: 978-0-486-78995-8.

[95] A. Gloden. *Mehrgradige Gleichungen*. 2nd edition. P. Noordhoff, Groningen, 1943.

[96] C. K. Goertz. “Dusty plasmas in the solar system”. In: *Rev. Geophys.* 27.2 (1989), p. 271.

[97] C. Goldbach. “Letter to Euler, July 18, 1750”. In: *Corresp. Math. Phys. (ed. Fuss)*. Vol. 1. http://eulerarchive.maa.org/correspondence/. St. Petersburg, 1843, pp. 525–526.

[98] R. Gordon, R. Bender, and G. T. Herman. “Algebraic reconstruction techniques (ART) for three-dimensional electron microscopy and x-ray photography”. In: *J. Theor. Biol.* 29.3 (1970), pp. 471–482.

[99] G. R. Grimmet. “At theorem about random fields”. In: *Bull. Lond. Math. Soc.* 5.1 (1973), pp. 81–84.

[100] P. Gritzmann. “On the reconstruction of finite lattice sets from their X-rays”. In: *Discrete Geometry for Computer Imagery*. Ed. by E. Ahronovitz and C. Fiorio. Springer, Berlin, 1997, pp. 19–32.

[101] P. Gritzmann and S. de Vries. “Reconstructing crystalline structures from few images under high resolution transmission electron microscopy”. In: *Mathematics: Key Technology for the Future*. Ed. by W. Jäger. Springer, Berlin, 2003, pp. 441–459.

[102] P. Gritzmann, B. Langfeld, and M. Wiegelmann. “Uniqueness in Discrete Tomography: Three Remarks and a Corollary”. In: *SIAM J. Discrete Math.* 25.4 (2011), pp. 1589–1599.

[103] C. W. Groetsch. *Inverse problems in the mathematical sciences*. Springer, Wiesbaden, 1993. ISBN: 978-3-322-99204-8.

[104] A. F. Gutsol and S. P. Gangoli. “Transverse 2-D Gliding Arc Modeling”. In: *IEEE Trans. Plasma Sci.* 45.4 (2017), pp. 555–564.

[105] X. Guyon. *Random Fields on a Network. Modelling, Statistics, and Applications*. Probability and its Applications. Springer, New York, 1995. ISBN: 978-0-387-94428-9.

[106] J. Hadamard. *Lectures on the Cauchy problem in linear partial differential equations*. Reprint of the 1923 original. Dover Publications Inc., Mineola, 1952. ISBN: 978-0-486-78148-8.

[107] V. Hadziavdic, F. Melandso, and A. Hanssen. “Particle tracking from image sequences of complex plasma crystals”. In: *Phys. Plasmas* 13.5 (2006), p. 053504.

[108] L. Hajdu and R. Tijdeman. “Algebraic aspects of discrete tomography”. In: *J. Reine Angew. Math.* 2001.534 (2001), pp. 119–128.

[109] J. M. Hammersley and P. Clifford. “Markov fields on finite graphs and lattices”. unpublished manuscript. 1968.

[110] G. H. Hardy and E. M. Wright. *An Introduction to the Theory of Numbers*. 6th edition. Oxford University Press, Oxford, 2008. ISBN: 0-19-853171-0.

[111] W. K. Hastings. “Monte Carlo sampling methods using Markov Chains and their applications”. In: *Biometrika* 57.1 (1970), pp. 97–109.

[112] Y. Hayashi, Y. Hirose, and Y. Seno. “Polycrystal orientation mapping using scanning three-dimensional X-ray diffraction microscopy”. In: *J. Appl. Crystallogr.* 48.4 (2015), pp. 1094–1101.

[113] A. Heppes. “On the determination of probability distributions of more dimensions by their projections”. In: *Acta Math. Acad. Sci. Hung.* 7.3-4 (1956), pp. 403–410.

[114] G. T. Herman. “Reconstruction of binary patterns from a few projections”. In: *International Computing Symposium 1973*. Ed. by A. Günther, B. Levrat, and H. Lipps. North-Holland, Amsterdam, 1974, pp. 371–378.

[115] G. T. Herman and A. Kuba, eds. *Advances in Discrete Tomography and its Applications*. Birkhäuser, Boston, 2007. ISBN: 978-0-8176-3614-2.

[116] G. T. Herman and A. Kuba, eds. *Discrete Tomography: Foundations, Algorithms, and Applications*. Birkhäuser, Boston, 1999. ISBN: 0-8176-4101-7.

[117] G. T. Herman and A. Lent. "Iterative reconstruction algorithms". In: *Comput. Biol. Med.* 6.4 (1976), pp. 273–294.

[118] S. Hernández and F. Luca. "Integer roots chromatic polynomials of nonchordal graphs and the Prouhet-Tarry-Escott problem". In: *Graph Combinator.* 21.3 (2005), pp. 319–323.

[119] R. Hovden, P. Ercius, Y. Jiang, D. Wang, Y. Yu, H. D. Abruña, V. Elser, and D. A. Muller. "Breaking the Crowther limit: Combining depth-sectioning and tilt tomography for high-resolution, wide-field 3D reconstructions". In: *Ultramicroscopy* 140.1 (2014), pp. 26–31.

[120] N. E. Hurt. *Phase Retrieval and Zero Crossings: Mathematical Methods in Image Reconstruction*. Kluwer Academic Publishers Group, Dordrecht, 1989. ISBN: 0-7923-0210-9.

[121] R. W. Irving and M. R. Jerrum. "Three-dimensional statistical data security problems". In: *SIAM J. Comput.* 23.1 (1994), pp. 170–184.

[122] E. Ising. "Beitrag zur Theorie des Ferromagnetismus". In: *Z. Phys.* 31.1 (1925), pp. 253–258.

[123] B. Jakobsen, H. F. Poulsen, U. Lienert, J. Almer, S. D. Shastri, H. O. Sorensen, C. Gundlach, and W. Pantleon. "Formation and subdivision of deformation structures during plastic deformation". In: *Science* 312.5775 (2006), pp. 889–892.

[124] P. Jaming. "Phase retrieval techniques for radar ambiguity problems". In: *J. Fourier Anal. Appl.* 5.4 (1999), pp. 309–329.

[125] I. T. Jolliffe. *Principal Component Analysis*. 2nd edition. Springer, New York, 2002. ISBN: 978-0-387-95442-4.

[126] J. Kaipio and E. Somersalo. *Statistical and computational inverse problems*. Springer, New York, 2006. ISBN: 0-387-22073-9.

[127] A. C. Kak and M. Slaney. *Principles of Computerized Tomographic Imaging*. Reprint of the 1988 original. Society for Industrial and Applied Mathematics (SIAM), Philadelphia, 2001. ISBN: 0-89871-494-X.

[128] E. Kamke. "Verallgemeinerungen des Waring-Hilbertschen Satzes". In: *Math. Ann.* 83.1-2 (1921), pp. 85–112.

[129] R. M. Karp. “Reducibility among combinatorial problems”. In: *Complexity of Computer Computations, (ed. by R.E. Miller and J.W. Thatcher)*. Plenum Press, New York, 1972, pp. 85–103.

[130] M. B. Katz. *Questions of Uniqueness and Resolution in Reconstruction from Projections*. Vol. 26. Lecture Notes in Biomathematics. Springer, Berlin, 1978. ISBN: 3-540-09087-8.

[131] H. Katz-Boon, C. J. Rossouw, M. Weyland, A. M. Funston, P. Mulvaney, and J. Etheridge. “Three-Dimensional Morphology and Crystallography of Gold Nanorods”. In: *Nano Lett.* 11.1 (2011), pp. 273–278.

[132] V. J. Keilis-Borok and T. B. Yanovskaya. “Inverse problems of seismology (structural review)”. In: *Geophys. J. Royal Astr. Soc.* 13.1-3 (1967), pp. 223–234.

[133] R. Kieft, K. Schreel, G. van der Plas, and C. Rindt. “The application of a 3D PTV algorithm to a mixed convection flow”. In: *Exp. Fluids* 33.4 (2002), pp. 603–611.

[134] M. Kiermaier. “Geometric Solutions of the Prouhet-Tarry-Escott Problem”. Student project thesis. Zentrum Mathematik: Technische Universität München, 2004.

[135] R. Kindermann and J. L. Snell. *Markov Random Fields and Their Applications*. AMS, Providence, 1980. ISBN: 0-8218-5001-6.

[136] A. King, G. Johnson, D. Engelberg, W. Ludwig, and J. Marrow. “Observations of intergranular stress corrosion cracking in a grain-mapped polycrystal”. In: *Science* 321.5887 (2008), pp. 382–385.

[137] H. Kleiman. “A note on the Tarry-Escott problem”. In: *J. Reine Angew. Math.* 1975.278-279 (1975), pp. 48–51.

[138] J. Klukowska, R. Davidi, and G. T. Herman. “SNARK09 - A software package for reconstruction of 2D images from 1D projections”. In: *Comput. Meth. Prog. Bio.* 110.3 (2013), pp. 424–440.

[139] H. Kohl and L. Reimer, eds. *Transmission Electron Microscopy*. Springer, Berlin, 2008. ISBN: 978-0-387-40093-8.

[140] S. Kolev and A. Bogaerts. “A 2D model for a gliding arc discharge”. In: *Plasma Sources Sci. Technol.* 24.1 (2015), p. 015025.

[141] T. Y. Kong and G. T. Herman. “On which grids can tomographic equivalence of binary pictures be characterized in terms of elementary switching operations?” In: *Int. J. Imaging Syst. Technol.* 9.2-3 (1998), pp. 118–125.

[142] S. Kongsiriwong and S. Prugsapitak. “On the number of solutions of the Tarry-Escott problem of degree two and the related problem over some finite fields”. In: *Period. Math. Hung.* 69.2 (2014), pp. 190–198.

[143] S. I. Krasheninnikov, R. D. Smirnov, and D. L. Rudakov. “Dust in magnetic fusion devices”. In: *Plasma Phys. Controlled Fusion* 53.8 (2011), p. 083001.

[144] A. Kumar, L. Nguyen, M. DeGraef, and V. Sundararaghavan. “A Markov random field approach for microstructure synthesis”. In: *Modelling Simul. Mater. Sci. Eng.* 24.3 (2016), p. 035015.

[145] F. Labelle and J. R. Shewchuk. “Anisotropic Voronoi diagrams and guaranteed-quality anisotropic mesh generation”. In: *SoCG 2003: Proceedings of the nineteenth annual symposium on Computational geometry*. ACM Press, 2003, pp. 191–200.

[146] C. Lautensack. “Random Laguerre Tessellations”. PhD thesis. Fakultät für Mathematik: Universität Karlsruhe, 2007.

[147] C. Lautensack and S. Zuyev. “Random Laguerre tessellations”. In: *Adv. Appl. Probab.* 40.3 (2008), pp. 630–650.

[148] D. H. Lehmer. “The Tarry-Escott problem”. In: *Scripta Math.* 13.1 (1947), pp. 37–41.

[149] E. Levitan, M. Chan, and G. T. Herman. “Image-modeling Gibbs priors”. In: *Graph. Model. Im. Proc.* 57.2 (1995), pp. 117–130.

[150] H. Li, N. Chawla, and Y. Jiao. “Reconstruction of heterogeneous materials via stochastic optimization of limited-angle X-ray tomographic projections”. In: *Scr. Mater.* 86.1 (2014), pp. 48–51.

[151] H. Li, S. Kaira, N. Chawla, and Y. Jiao. “Accurate stochastic reconstruction of heterogeneous microstructures by limited x-ray tomographic projections”. In: *J. Microsc.* 264.3 (2016), pp. 339–350.

[152] Y. Lia, F. Qian, J. Xiang, and C. M. Lieber. “Nanowire electronic and opto-electronic devices”. In: *Mater. Today* 9.10 (2006), pp. 18–27.

[153] H. Y. Liao and G. T. Herman. “Automated estimation of the parameters of Gibbs priors to be used in binary tomography”. In: *Discrete Appl. Math.* 139.1-3 (2004), pp. 149–170.

[154] V. L. Lo and R. P. Millane. “Reconstruction of compact binary images from limited Fourier amplitude data”. In: *J. Opt. Soc. Am. A* 25.10 (2008), pp. 2600–2607.

[155] G. G. Lorentz. “A problem of plane measure”. In: *Amer. J. Math.* 71.2 (1949), pp. 417–426.

[156] W. Ludwig, S. Schmidt, E. M. Lauridsen, and H. F. Poulsen. "X-ray diffraction contrast tomography: A novel technique for three-dimensional grain mapping of polycrystals. I. Direct beam case". In: *J. Appl. Crystallogr.* 41.2 (2008), pp. 302–309.

[157] A. Lyckegaard, A. Alpers, W. Ludwig, R. W. Fonda, L. Margulies, A. Götz, H. O. Sørensen, S. R. Dey, H. F. Poulsen, and E. M. Lauridsen. "3D grain reconstruction from boxscan data". In: *Proc. of the 31th Risø Int. Symp. on Materials Science*. 2010, pp. 329–336.

[158] A. Lyckegaard, E. M. Lauridsen, W. Ludwig, R. W. Fonda, and H. F. Poulsen. "On the use of Laguerre Tessellations for representations of 3D grain structures". In: *Adv. Eng. Mater.* 13.3 (2011), pp. 165–170.

[159] A. Madsen. *Conceptual design report: Scientific instrument MID*. Tech. rep. http://bib-pubdb1.desy.de/record/95100/files/TR-2011-008-CDR_WP83_2012-01-02.pdf?version=3. XFEL.EU TR-2011-008, 2011.

[160] J. D. Malone, M. T. El-Haddad, I. Bozic, L. A. Tye, L. Majeau, N. Godbout, A. M. Rollins, C. Boudoux, K. M. Joos, S. N. Patel, and Y. K. Tao. "Simultaneous multimodal ophthalmic imaging using swept-source spectrally encoded scanning laser ophthalmoscopy and optical coherence tomography". In: *Biomed. Opt. Express* 8.1 (2017), pp. 193–206.

[161] R. Maltby. "A combinatorial identity of subset-sum powers in rings". In: *Rocky Mountain J. Mat.* 30.1 (2000), pp. 325–329.

[162] R. Maltby. "Pure product polynomials and the Prouhet-Tarry-Escott problem". In: *Math. Comp.* 66.219 (1997), pp. 1323–1340.

[163] L. Margulies, G. Winther, and H. F. Poulsen. "In situ measurement of grain rotation during deformation of polycrystals". In: *Science* 291.5512 (2001), pp. 2392–2394.

[164] L. Martí-Bonmatí, R. Sopena, P. Bartumeus, and P. Sopena. "Multimodality imaging techniques". In: *Contrast Media Mol. Imaging* 5.4 (2010), pp. 180–189.

[165] J. Matoušek, A. Přívětivý, and P. Škovroň. "How many points can be reconstructed from k projections?" In: *SIAM J. Discrete Math.* 22.4 (2008), pp. 1605–1623.

[166] J. McLaughlin. "An indentity motivated by an amazing identity of Ramanujan". In: *Fibonacci. Quart.* 48.34-38 (2010), pp. 34–38.

[167] A. Melling. "Tracer particles and seeding for particle image velocimetry". In: *Meas. Sci. Technol.* 8.12 (1997), pp. 1406–1416.

[168] Z. A. Melzak. "A note on the Tarry-Escott problem". In: *Canad. Math. Bull.* 4.3 (1961), pp. 233–237.

[169] N. Metropolis, A. W. Rosenbluth, M. N. Rosenbluth, A. H. Teller, and E. Teller. "Equation of state calculations by fast computing machines". In: *J. Chem. Phys.* 21.6 (1953), pp. 1087–1092.

[170] N. Metropolis and S. Ulam. "The Monte Carlo method". In: *J. Amer. Stat. Assoc.* 44.247 (1949), pp. 335–341.

[171] P. A. Midgley and R. E. Dunin-Borkowski. "Electron tomography and holography in materials science". In: *Nature Mater.* 8.4 (2009), pp. 271–280.

[172] M. Mignotte and D. Ştefănescu. *Polynomials: An algorithmic approach.* Springer, Singapore, 1999. ISBN: 978-9814021517.

[173] R. P. Millane. "Phase retrieval in crystallography and optics". In: *J. Opt. Soc. Am. A* 7.3 (1990), pp. 394–411.

[174] G. Möbus and B. J. Inkson. "Nanoscale tomography in materials science". In: *Mater. Today* 10.12 (2007), pp. 18–25.

[175] S. Mokkapati and C. Jagadish. "III-V compound SC for optoelectronic devices". In: *Mater. Today* 12.4 (2009), pp. 22–32.

[176] G. Myerson. "How small can a sum of roots of unity be?" In: *Amer. Math. Monthly* 93.6 (1986), pp. 457–459.

[177] F. Natterer. *The Mathematics of Computerized Tomography.* Reprint of the 1986 original. Society for Industrial and Applied Mathematics (SIAM), Philadelphia, 2001. ISBN: 0-89871-493-1.

[178] H. D. Nguyen. "A new proof of the Prouhet-Tarry-Escott problem". In: *Integers* 16.A1 (2016), pp. 1–9.

[179] J. E. Nymann. "On the probability that k positive integers are relatively prime". In: *J. Number Theor.* 4.5 (1972), pp. 469–473.

[180] S. E. Offerman, N. H. van Dijk, J. Sietsma, S. Grigull, E. M. Lauridsen, L. Margulies, H. F. Poulsen, M. T. Rekveldt, and S. van der Zwaag. "Grain nucleation and growth during phase transformations". In: *Science* 298.5595 (2002), pp. 1003–1005.

[181] O. Öktem. "Mathematics of Electron Tomography". In: *Handbook of Mathematical Methods in Imaging.* Ed. by O. Scherzer. 2nd edition. Springer, New York, 2015, pp. 937–1031.

[182] N. P. Oxtoby, E. J. Griffith, C. Durniak, J. F. Ralph, and D. Samsonov. "Ideal Gas Behavior of a Strongly Coupled Complex (Dusty) Plasma". In: *Phys. Rev. Lett.* 111.1 (2013), p. 015002.

[183] X. Pan, E. Y. Sidky, and M. Vannier. "Why do commercial CT scanners still employ traditional, filtered back-projection for image reconstruction?" In: *Inverse Probl.* 25.12 (2009), p. 123009.

[184] P. A. Panzone. “On a formula of S. Ramanujan”. In: *Amer. Math. Monthly* 122.1 (2015), pp. 65–69.

[185] C. H. Papadimitriou and K. Steiglitz. *Combinatorial Optimization: Algorithms and Complexity*. Dover Publications Inc., Mineola, 1998. ISBN: 0-486-40258-4.

[186] A. D. Parsons, S. W. T. Price, N. Wadeson, M. Basham, A. M. Beale, A. W. Ashton, J. F. W. Mosselmans, and P. D. Quinn. “Automatic processing of multimodal tomography datasets”. In: *J. Synchrotron Rad.* 24.1 (2017), pp. 248–256.

[187] S. Pellerin, J. Richard F. Chapelle, J. M. Cormier, and K. Musiol. “Heat string model of bi-dimensional dc Glidarc”. In: *J. Phys. D: Appl. Phys.* 33.19 (2000), pp. 2407–2419.

[188] R. S. Pennington, S. König, A. Alpers, C. B. Boothroyd, and R. E. Dunin-Borkowski. “Reconstruction of an InAs nanowire using geometric and algebraic tomography”. In: *Journal of Physics: Conference Series*. Vol. 326. 2011, 012045 (4 pp.)

[189] F. Pereira, H. Stüer, E. C. Graff, and M. Gharib. “Two-frame 3D particle tracking”. In: *Meas. Sci. Technol.* 17.7 (2006), pp. 1680–1692.

[190] R. B. Potts. “Some generalized order-disorder transitions”. In: *Proc. Camb. Phil. Soc.* 48.1 (1952), pp. 106–109.

[191] H. F. Poulsen. “An introduction to three-dimensional X-ray diffraction microscopy”. In: *J. Appl. Crystallogr.* 45.6 (2012), pp. 1084–1097.

[192] H. F. Poulsen. *Three-Dimensional X-ray Diffraction Microscopy*. Springer, Berlin, 2004. ISBN: 3-540-22330-4.

[193] H. F. Poulsen and X. Fu. “Generation of grain maps by an algebraic reconstruction technique”. In: *J. Appl. Crystallogr.* 36.4 (2003), pp. 1062–1068.

[194] H. F. Poulsen, S. Schmidt, D. Juul Jensen, H. O. Sørensen, E. M. Lauridsen, U. L. Olsen, W. Ludwig, A. King, J. P. Wright, and G. B. M. Vaughan. “3D X-Ray Diffraction Microscopy”. In: *Strain and Dislocation Gradients from Diffraction: Spatially-Resolved Local Structure and Defects*. Ed. by R. Barabash and G. Ice. World Scientific, Singapore, 2014, pp. 205–253.

[195] F. Press. “Earth models obtained by Monte-Carlo inversion”. In: *J. Geophys. Res.* 73.16 (1968), pp. 5223–5234.

[196] L. Priester. *Grain Boundaries: From Theory to Engineering*. Springer, Dordrecht, 2013. ISBN: 978-94-007-4968-9.

[197] M. E. Prouhet. “Mémoire sur quelques relations entre les puissances des nombres”. In: *C. R. Math. Acad. Sci. Paris* 33 (1851), p. 225.

[198] S. Prugsapitak. “The Tarry-Escott problem of degree two”. In: *Period. Math. Hung.* 65.1 (2012), pp. 157–165.

[199] S. Prugsapitak. “The Tarry-Escott problem of degree two over quadratic fields”. In: *East-West J. Math.* 1.1 (2010), pp. 306–316.

[200] S. Prugsapitak. “The Tarry-Escott problem over quadratic fields”. PhD thesis. Department of Mathematics: University of Illinois at Urbana-Champaign, 2009.

[201] J. Radon. “Über die Bestimmung von Funktionen durch ihre Integralwerte längs gewisser Mannigfaltigkeiten”. In: *Ber. Sächs. Akad. Wiss. Leipzig, Math. Phys. Kl.* 69.1 (1917), pp. 262–277.

[202] P. Reischig, A. King, L. Nervo, N. Viganò, Y. Guilhem, W. J. Palenstijn, K. J. Batenburg, M. Preuss, and W. Ludwig. “Advances in X-ray diffraction contrast tomography: flexibility in the setup geometry and application to multiphase materials”. In: *J. Appl. Crystallogr.* 46.2 (2013), pp. 297–311.

[203] A. Rényi. “On projections of probability distributions”. In: *Acta Math. Acad. Sci. Hungar.* 3.3 (1952), pp. 131–142.

[204] D. Reuss, R. Adrian, and C. Landreth. “Two-Dimensional Velocity Measurements in a Laminar Flame Using Particle Image Velocimetry”. In: *Combust. Sci. Technol.* 67.4-6 (1986), pp. 73–83.

[205] J. Reyes-Gasga, J. L. Elechiguerra, C. Liu, A. Camacho-Bragado, J. M. Montejano-Carrizales, and M. Jose Yacaman. “On the structure of nanorods and nanowires with pentagonal cross-sections”. In: *J. Cryst. Growth* 286.1 (2006), pp. 162–172.

[206] F. Richard, J. M. Cormier, S. Pellerin, and J. Chapelle. “Physical study of a gliding arc discharge”. In: *J. Appl. Phys.* 79.5 (1996), pp. 2245–2250.

[207] C. Robert and G. Casella. “A Short History of Markov Chain Monte Carlo: Subjective Recollections from Incomplete Data”. In: *Statist. Sci.* 26.1 (2011), pp. 102–115.

[208] L. Rodek. “Application of Discrete Tomographic Methods in Nondestructive Testing and Materials Science”. PhD thesis. Department of Image Processing and Computer Graphics: University of Szeged, 2015.

[209] L. Rodek, H. F. Poulsen, E. Knudsen, and G. T. Herman. “A stochastic algorithm for reconstruction of grain maps of moderately deformed specimens based on X-ray diffraction”. In: *J. Appl. Crystallogr.* 40.2 (2007), pp. 313–321.

[210] H. J. Ryser. “Combinatorial properties of matrices of zeros and ones”. In: *Canad. J. Math.* 9.1 (1957), pp. 371–377.

[211] S. Schmidt, S. F. Nielsen, C. Gundlach, L. Margulies, X. Huang, and D. Juul Jensen. “Watching the growth of bulk grains during recrystallization of deformed metals”. In: *Science* 305.5681 (2004), pp. 229–232.

[212] M. J. Schrapp and G. T. Herman. “Data fusion in X-ray computed tomography using a superiorization approach”. In: *Rev. Sci. Instrum.* 85.5 (2014), p. 053701.

[213] A. Schrijver. *Theory of Linear and Integer Programming*. Wiley, Chichester, 1986. ISBN: 0-471-90854-1.

[214] J. A. Schwartz, M. Kumar, B. L. Adams, and D. P. Field, eds. *Electron Backscatter Diffraction in Materials Science*. 2nd edition. Springer, New York, 2009. ISBN: 978-0-387-88135-5.

[215] C.-C. Scott M. C. and Chen, M. Mecklenburg, C. Zhu, R. Xu, P. Ercius, U. Dahmen, B. C. Regan, and J. Miao. “Electron tomography at 2.4-ångström resolution”. In: *Nature* 483.7390 (2012), pp. 444–447.

[216] O. Šedivý, T. Brereton, D. Westhoff, L. Polívka, V. Beneš, V. Schmidt, and A. Jäger. “3D reconstruction of grains in polycrystalline materials using a tessellation model with curved grain boundaries”. In: *Phil. Mag.* 96.18 (2016), pp. 1926–1949.

[217] O. Šedivý, J. Dake, C. E. Krill III, V. Schmidt, and A. Jäger. “Description of the 3D morphology of grain boundaries in aluminum alloys using tessellation models generated by ellipsoids”. In: *Image Anal. Stereol.* 36.1 (2017), pp. 5–13.

[218] A. Shliferstein and Y. T. Chien. “Switching components and the ambiguity problem in the reconstruction of pictures from their projections”. In: *Pattern Recogn.* 10.5-6 (1978), pp. 327–340.

[219] T. N. Sinha. “A note on a theorem of Lehmer”. In: *J. London Math. Soc.* s2-4.3 (1972), pp. 541–544.

[220] T. N. Sinha. “A relation between the coefficients and roots of two equations and its application to diophantine problems”. In: *J. Res. Nat. Bur. Standards Sect. B* 74B (1970), pp. 31–36.

[221] C. H. Slump and J. J. Gerbrands. “A network flow approach to reconstruction of the left ventricle from two projections”. In: *Comput. Vision. Graph.* 18.1 (1982), pp. 18–36.

[222] A. F. M. Smith and G. O. Roberts. “Bayesian computation via the Gibbs sampler and related Markov chain Monte Carlo methods”. In: *J. R. Statist. Soc. B* 55.1 (1993), pp. 3–23.

[223] A. Spettl, T. Brereton, Q. Duan, T. Werz, C. E. Krill III, D. P. Kroese, and V. Schmidt. “Fitting Laguerre tessellation approximations to tomographic image data”. In: *Phil. Mag.* 96.2 (2016), pp. 166–189.

[224] F. C. R. Spieksma and G. J. Woeginger. “Geometric three-dimensional assignment problems”. In: *European J. Oper. Res.* 91.3 (1996), pp. 611–618.

[225] R. M. Suter, D. Hennessy, C. Xiao, and U. Lienert. “Forward modeling method for microstructure reconstruction using X-ray diffraction microscopy: Single-crystal verification”. In: *Rev. Sci. Instr.* 77.12 (2006), p. 123905.

[226] I. Svalbe and S. Chandra. “Growth of discrete projection ghosts created by iteration”. In: *Discrete geometry for computer imagery*. Vol. 6607. Lecture Notes in Comput. Sci. Springer, Heidelberg, 2011, pp. 406–416.

[227] I. Svalbe, N. Nazareth, N. Normand, and S. Chandra. “On Constructing Minimal Ghosts”. In: *2010 International Conference on Digital Image Computing: Techniques and Applications*. IEEE, Los Alamitos, 2010, pp. 276–281.

[228] I. Svalbe and N. Normand. “Properties of minimal ghosts”. In: *Discrete geometry for computer imagery*. Vol. 6607. Lecture Notes in Comput. Sci. Springer, Heidelberg, 2011, pp. 417–428.

[229] A. Tarantola. *Inverse Problem Theory and Methods for Model Parameter Estimation*. SIAM, Philadelphia, 2005. ISBN: 978-0-898715-72-9.

[230] G. Tarry. “Question 4100”. In: *Interméd. Math.* 19.1 (1912). (Answers to the question were given by E. Barbette, E. Miot, and Welsch in 20.1 (1913), pp. 68-70), p. 200.

[231] K. Teferra and L. Graham-Brady. “Tessellation growth models for polycrystalline microstructures”. In: *Comput. Mater. Sci.* 102.1 (2015), pp. 57–67.

[232] L. Tierney. “Markov chains for exploring posterior distributions”. In: *Ann. Statistics* 22.4 (1994), pp. 1701–1762.

[233] S. Van Aert, K. J. Batenburg, M. D. Rossell, R. Erni, and G. Van Tendeloo. “Three-dimensional atomic imaging of crystalline nanoparticles”. In: *Nature* 470.7334 (2011), pp. 374–376.

[234] M. N. M. van Lieshout. “An introduction to planar random tessellation models”. In: *Spatial Statistics* 1.1 (2012), pp. 40–49.

[235] E. Vardi, G. T. Herman, and T. Y. Kong. “Speeding up stochastic reconstructions of binary images from limited projection directions”. In: *Linear Algebra Appl.* 339.1-3 (2012), pp. 75–89.

[236] N. Viganò, W. Ludwig, and K. J. Batenburg. “Reconstruction of local orientation in grains using a discrete representation of orientation space”. In: *J. Appl. Crystallogr.* 47.6 (2014), pp. 1826–1840.

[237] J. B. Wagner, N. Sköld, L. R. Wallenberg, and L. Samuelson. “Growth and segregation of GaAs-$Al_xIn_{1-x}P$ core-shell nanowires”. In: *J. Cryst. Growth* 312.10 (2010), pp. 1755–1760.

[238] B. Wieneke. “Iterative reconstruction of volumetric particle distribution”. In: *Meas. Sci. Technol.* 24.2 (2013), p. 024008.

[239] G. Winkler. *Image Analysis, Random Fields and Markov Chain Monte Carlo Methods*. 2nd edition. Springer, Berlin, 2006. ISBN: 3-540-44213-8.

[240] E. M. Wright. "An easier Waring's problem". In: *J. London Math. Soc.* 9.4 (1934), pp. 267–272.

[241] E. M. Wright. "On Tarry's problem (I)". In: *Q. J. Math.* 6.1 (1935), pp. 261–267.

[242] E. M. Wright. "Prouhet's 1851 Solution of the Tarry-Escott Problem of 1910". In: *Amer. Math. Monthly* 66.3 (1959), pp. 199–201.

[243] E. M. Wright. "The Tarry-Escott and the "easier" Waring problem". In: *J. Reine Angew. Math.* 1979.309 (1979), pp. 170–173.

[244] X. Wu, Y. Wu, C. Zhang, G. Li, Q. Huang, L. Chen, K. Qiu, H. Zhou, and K. Cen. "Fundamental research on the size and velocity measurements of coal powder by trajectory imaging". In: *J. Zhejiang Univ. Sci. A* 14.5 (2013), pp. 377–382.

[245] A. Zhang, G. Zheng, and C. Lieber. *Nanowires: Building Blocks for Nanoscience and Nanotechnology*. Springer, Berlin, 2016. ISBN: 978-3-319-41979-4.

[246] J. Zhu. "Optical Diagnostics of Non-thermal Plasmas and Plasma-assisted Combustion". PhD thesis. Division of Combustion Physics: Lund University, 2015.

[247] S. Zopf. "Construction of switching components". In: *Discrete geometry for computer imagery*. Vol. 4245. Lecture Notes in Comput. Sci. Springer, Berlin, 2006, pp. 157–168.

Index

1-In-3-SAT, 24
3-dimensional X-ray diffraction (3DXRD), 7
3DXRD, 7
3-color tomography, 30

$B_k(j_1, j_2)$, 23
$C(m, n, k)$, 23
$\mathbb{H}$, 6
$\mathbb{K}$, 6
$\mathrm{lin}(v)$, 6
$\mathbb{NP}$, 6
$O(n)$, 6
$\mathbb{P}$, 6
$P(k, a)$, 28
$\mathrm{pat}_k(x, j_1, j_2)$, 28
$\mathbb{Z}[i]$, 6

Algebraic Reconstruction Technique (ART), 39
algorithm
  Algorithm I, 45
  Algorithm II, 45
  ART, 39
  filtered backprojection, 46
  GKXR, 47
  HIO, 45
  linear programming, 35
  MART, 30
  Metropolis, 42
  Metropolis-based Monte Carlo, 45
  MPW, 47
ART, 39
artefacts
  missing wedge, 46
  non-linear projection intensities, 46

binary
  solutions, 30
  superposed phase retrieval, 44
block constraints, 22, 29
blocks, 23, 27
Boltzmann distribution, 40
Boolean formula, 24
box, 23

candidate grid, 31
candidate points, 31
center-of-mass (CMS), 35
chemistry, 6
clustering, 35
CMS, 35
coherent X-rays, 43
combinatorial models, 27
computer science, 6
$\textsc{Consistency}_{\mathcal{F}^d}(S_1, \ldots, S_m)$, 20
convex lattice sets, 20

DCT, 7
deformed, 35
diffraction contrast tomography (DCT), 7
discrete
  inverse problem, 27
  optimization problem, 32
  tomography, 18, 24, 26, 46
displacement field, 26
double-resolution, 24
DR, 24
dynamic discrete tomography, 26, 32

easier Waring problem, 10
EBSD, 37
electron backscatter diffraction (EBSD), 37
electron tomography (ET), 46
ellipsoidal norm, 36
error correction, 18, 19
ESRF, 7
ET, 46

European synchrotron radiation facility (ESRF), 7
European X-ray free-electron laser (European XFEL), 6

filtered backprojection, 46
free-electron laser, 6

GBPD, 35
generalized balanced power cell, 36
generalized balanced power diagrams (GBPDs), 35
geometric tomography, 46
Gerchberg-Saxton scheme, 46
Gibbs
    priors, 40
GKXR, 47
gliding arc discharge, 33
grain map, 7, 35
grains, 7, 35
    moderately deformed, 39
    undeformed, 39

HAADF STEM, 46
Hammersley-Clifford theorem, 40
high-angle annular dark-field scanning transmission electron microscopy (HAADF STEM), 46
Hilbert-Kamke problem, 10
Hybrid-Input-Output (HIO), 45

ill-posed, 18
incoherent X-rays, 45
interchanges, 24
inverse crimes, 41
Ising model, 40

Johnson–Mehl, 39

ℓ_1-norm, 19
Laguerre random tessellations, 39
lattice
    $\mathcal{L}$-gon, 15
    lines, 11
    sets, 11
likelihood function, 41
linear optimization problem, 36
linear program, 35
local switches, 24

Markov
    chain, 42
    Chain Monte Carlo, 42
    random field, 40
    -type property, 26
MART, 30
Materials Imaging and Dynamics (MID), 6
materials science, 6, 35
MCMC, 42
Metropolis-based Monte Carlo methods, 45
microparticles, 7
MID, 6
minimum weight perfect bipartite matching, 26
MPW, 47
multiplicative algebraic reconstruction technique (MART), 30

nanoscience, 6
nanowires, 7
$\textsc{nDR}(\varepsilon)$, 24
$\textsc{Nearest-Solution}_{\mathcal{F}^d}(S_1, \ldots, S_m)$, 21
Newton identities, 20
noise compensation, 18
$\textsc{nSR}(k, \varepsilon)$, 23

orientation map, 35

particle tracking, 26
particle tracking velocimetry (PTV), 30
pattern constraints, 29
phase retrieval problem, 43

binary, 43
binary superposed, 44
physics, 6
plasma column, 33
Poisson–Voronoi, 38
polycrystal, 7
polycrystalline materials, 7
Potts model, 40
principal component analysis, 37
prior distribution, 40
problem
1-In-3-SAT, 24
3-color tomography, 30
3D-Matching, 27
Consistency$_{\mathcal{F}^d}(S_1, \ldots, S_m)$, 20
DR, 24
easier Waring, 10
Hilbert-Kamke, 10
linear optimization, 36
nDR(ε), 24
Nearest-Solution$_{\mathcal{F}^d}(S_1, \ldots, S_m)$, 21
nSR(k, ε), 23
phase retrieval, 43
binary superposed, 44
PTE, 8
PTE$_d$, 10
R-PTE, 11
Similar-Solution$_{\mathcal{F}^d}(S_1, \ldots, S_m)$, 21
tomographic point tracking, 26
Uniqueness$_{\mathcal{F}^d}(S_1, \ldots, S_m)$, 21
weight-balanced least-squares assignment, 36
X-Ray-Correction$_{\mathcal{F}^d}(S_1, \ldots, S_m)$, 21
Prouhet-Tarry-Escott problem (*see PTE problem*), 8
PTE problem, 8
solution
equivalent, 9
for (k, n), 8
ideal, 9
PTE$_d$ problem, 10
PTV, 30

quaternions, 39, 42

R-PTE problem, 11
Radon transform, 46
finite, 18
random tessellation models, 39
reduced solutions, 24
Riemann zeta function, 16
rolling horizon approach, 31, 32

second-order moments, 35
Similar-Solution$_{\mathcal{F}^d}(S_1, \ldots, S_m)$, 21
slip velocity, 33
stability, 18
stationary distribution, 42
stationary marked Poisson processes, 39
stochastic geometry, 38
super-resolution, 22, 23
support function, 47
switching component
m-switching component (in $\mathbb{K}^d$), 11
synchrotron, 7

TEM, 46
tessellation, 35
theorem
Frolov, 9
Gardner and Gritzmann, 20
Hammersley-Clifford, 40
Prouhet, 13
Rényi, 16, 20
tomographic point tracking, 26
partially tomographic case, 26
positionally determined case, 26
totally tomographic case, 26
tomographically equivalent

(with respect to $S_1, \ldots, S_m \in \mathcal{S}^d$), 11
tomography
discrete, 46
geometric, 46
totally unimodular, 30, 37
tracer particles, 7
tracking, 26
transition probabilities, 42
transmission electron microscope (TEM), 46

Uniqueness$_{\mathcal{F}^d}(S_1, \ldots, S_m)$, 21
unit quaternions, 39, 42
volume, 35

weight-balanced least-squares assignment problem, 37
windows, 27

X-ray
coherent, 43
incoherent, 45
of F parallel to S, 11
transform, 46
X-Ray-Correction$_{\mathcal{F}^d}(S_1, \ldots, S_m)$, 21
XFEL, 6